Fast Traction Control of Rovers on Prescribed Dynamic Trajectories with Wheel-Fighting Consideration

Mohammadreza Mottaghi, Robin Chhabra, *Member, IEEE*, Wei Huang

***Abstract*—To reliably localize and control wheeled autonomous rovers, their controllers must keep the wheels away from traction loss. In this paper, we develop a fast and practical traction control system for rovers that track dynamic trajectories on rough firm terrains, leveraging their normally existing redundant control directions. Trajectory-tracking performance is guaranteed by input-output linearizing a nonholonomic model of the system and employing an appropriate stabilizing control law. We propose a novel methodology to optimally lift the control signals at the rover's output level to determine the control actions that enhance the system's traction without affecting the tracking performance. The methodology uses the knowledge of wheels' friction coefficients and estimation of normal and tractive forces based on a nonholonomic rover model to optimally distribute the tractive forces among the wheels. The novelty is in redefining the optimization problem in both lateral and longitudinal directions that require minimum information about wheel-ground interactions and leads to linear optimality conditions. We define the notion of total required force/moment at system's center of mass to (i) introduce reference directions for tractive forces in the proposed cost functions, and (ii) identify the rover wheels fighting against the motion. To prevent wheel-fighting, we find sub-optimal solutions that suppress tractive forces at the fighting wheels. The proposed traction control system is implemented on a six-wheel autonomous Lunar rover and its efficacy is investigated by a developed software-in-the-loop simulation environment using Vortex Studio. This software simulates a 3-dimensional digital twin of the system, with different terrain and tire model options. When compared to the conventional pseudo-inverse solution, the developed traction controller demonstrates improved overall traction and it saves the rover from traction loss.**

***Index Terms*—Dynamic traction control, Output-tracking control, Optimal control, Wheel-fighting, Autonomous rovers.**

I. Introduction

TRACTION is one of the main concerns in the control of autonomous rovers/vehicles. Deprived traction results in losing mobility and stability of control system, deteriorating tracking performance, and erroneous wheel odometry for localization [1]. Traction is particularly crucial when a rover undergoes dynamic motions on rough terrains and planetary surfaces with lower gravity [2]. In this paper, the term *dynamic traction* is used to refer to maintaining close-to-zero-velocity condition at wheel-ground contact points during tracking a dynamic prescribed trajectory, i.e., respecting normally-imposed nonholonomic constraints. Accordingly, *dynamic traction control* means producing control inputs considering the dynamic traction on rough terrains. A dynamic traction controller must be real-time and have no influence on the tracking performance of the system.

The evolution of traction control systems for wheeled vehicles initiated in 1980s when different supervisory control strategies including anti-lock braking systems and anti-spin acceleration systems were proposed for commercialized vehicles [3]. For autonomous systems, traction control strategies have been developed based on wheel slippage estimation, using, e.g., tire deformation models [4], inertia measurement unit [5]–[9], and visual odometry [10], [11]. Such estimations not only can improve localization, but they also can be used in designing traction controllers [12]–[15]. Traction control algorithms working based on slippage estimation are divided into two categories: velocity-based and torque-based. In the former category, the estimated amount of slippage is compensated with appropriate speed commands [16], [17]. Since the system's dynamics is not directly involved in the computation of control commands, such approaches lead to incoordination between wheels (wheel-fighting) [18], [19]. In the latter category, slippage is included in the dynamics of the system and it is compensated by applying appropriate control torque commands. For example in [20], [21], the average slip ratio is defined as a control target and it is maintained in an optimal region using sliding mode control. Slippage dynamics can be also approximated [22], [23] and controlled applying an input-output linearizing feedback transformation [24].

Due to the lack of accurate models for wheel slippage [25], [26], several traction control algorithms with minimal dependency on slip estimation have been introduced. Iagnemma *et al*. propose a traction controller under the quasi-static assumption for planetary rovers. They employ redundant control actions to offer an optimal force distribution minimizing the ratio of tractive to normal reaction forces, known as *tractive ratios* [27]. This method is improved by introducing an enhanced quasi-static model independent of complex tire-soil interaction phenomenon for a rover named SOLERO [28]. For systems operating with high velocities, Sarkar *et al*. propose a torque-based traction control exploiting the redundancy in a mobile robot with two driven wheels and two active steering systems. They asymmetrically distribute the control torques when one wheel runs into a less desirable terrain condition. Their method is based on a primitive model of the system and relies on the wheels' slip curves only in the

M.R. Mottaghi and R. Chhabra are with the Mechanical and Aerospace Engineering department, Carleton University, Ottawa, Canada (e-mail: mohammadreza.mottaghi@carleton.ca, robin.chhabra@carleton.ca. W.Huang is with National Research Council of Canada (NRC-CNRC) AST center, Ottawa, Canada (e-mail: Wei.Huang@nrc-cnrc.gc.ca)

longitudinal direction [29]. Another dynamic traction control strategy for redundant autonomous rovers is proposed in [30], where a rigid body dynamical model of the system and a terramechanics model are combined to introduce an optimal control distribution to maximize traction. This approach is enhanced by redefining the optimization criterion to consider the quadratic norm of tractive ratios [31].

In the mentioned studies, complex terramechanics models [32] or accelerometers at wheels [33] are often necessary to compute control torques based on the knowledge of optimal tractive forces obtained using constraint-free dynamical models. However, the real-time estimation of terramechanic parameters is computationally demanding and not accurate, and accelerometer signals are known to be noisy. Further, the developed traction controllers are normally either based on simplistic vehicle models, or rely on numerical solutions of nonlinear optimizations, impeding their real-time implementation during dynamic tasks. To the best of the authors' knowledge, wheel-fighting phenomenon is also an understudied subject in the existing optimal dynamic traction control strategies. Wheel-fighting results in deterioration of traction and increase of the power consumption in the system.

In this paper, employing redundant control directions, an optimal distribution of control actions is proposed to enhance the dynamic traction of autonomous rovers, without affecting their tracking performance. The major contributions of this paper are as follows:

1) We propose a cost function resulting in a set of linear necessary conditions of optimality with respect to the optimization variable. Accordingly, the computation of the optimal distribution is fast and can be implemented in real-time dynamic applications.
2) We simultaneously consider the traction optimization in both longitudinal and lateral directions of the rover on arbitrary trajectories.
3) Under some explained assumptions, we use Lagrange-d'Alembert equations of motion for nonholonomic systems to approximate the tractive forces and normal ground reaction forces at the wheels. Accordingly in the developed dynamic traction controller, the dependency on the terrain and tire parameters is significantly reduced and only an approximation of the wheels' static friction coefficients is required.
4) We introduce the notion of the total required force and moment at system's center of mass dictated by the output-tracking control system. This concept is used to address the wheel-fighting problem by introducing a sub-optimal solution killing fighting tractive forces.

The outline of the paper is as follows. In Section II, we state the dynamic traction control problem that is considered in this paper. We propose a dynamic traction controller in Section III. Finally, the developed methodology is implemented on a six-wheel autonomous Lunar rover and its efficacy is investigated using a software-in-the-loop simulation environment in Section IV. Section V provides some concluding remarks.

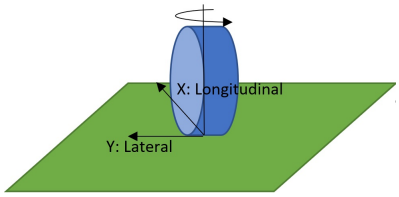

Fig. 1: The non-spinning local wheel coordinate frame

II. Problem Statement

A. Rover Model

In this paper, autonomous rovers with planar motion are modeled as mechanical control systems whose motion is restricted by tractive constraints in Pfaffian form. Tractive constraints refer to those corresponding to the zero-velocity conditions at wheel-ground contact points. We assume that non-tractive constraints (e.g., Ackerman constraints) are all holonomic and they have already been integrated [34]. We denote a configuration of the rover by the vector $\mathbf{q} \in \mathbb{R}^{\mathfrak{n}}$ such that $\mathbf{q} = [\mathbf{q}_1^T \ \mathbf{q}_2^T]^T$, where $\mathbf{q}_1 = [x_b, \ y_b, \ \theta]^T \in \mathbb{R}^3$ includes the position of the main body coordinate frame expressed in the inertial frame ($[x_b, \ y_b]^T$) and its rotation (θ), and $\mathbf{q}_2 \in \mathbb{R}^{\mathfrak{n}-3}$ includes the wheels' rotation and steering angles. If the number of the wheels is $\mathfrak{g}$, then the rover has $\mathfrak{n} - \mathfrak{g} - 3$ independent steering degrees freedom. Then, the vectors $[\mathbf{q}^T \ \dot{\mathbf{q}}^T]^T \in \mathbb{R}^{2\mathfrak{n}}$ form the state space of the system. We consider $\mathfrak{m}$ linearly independent tractive constraints in the following form:

$$A(\mathbf{q})\dot{\mathbf{q}} = \mathbb{O}_{\mathfrak{m}\times 1}, \tag{1}$$

where $A : \mathbb{R}^{\mathfrak{n}} \to \mathbb{R}^{\mathfrak{m}\times\mathfrak{n}}$ is the constraint matrix and $\mathbb{O}$ denotes the matrix of zeros with proper dimensions. Each row of A is a row vector whose multiplication with $\dot{\mathbf{q}}$ is the velocity of a wheel-ground contact point in the longitudinal or lateral direction of the wheel. The directions are specified with respect to a non-spinning local wheel coordinate frame at the wheel-ground contact point that rotates with the wheel in the yaw direction (see Fig.1). Based on the Lagrange-d'Alembert principle, the matrix form of the governing equations of motion on Q can be formulated as

$$\begin{aligned} &\dot{\mathbf{q}} = N(\mathbf{q})\boldsymbol{\eta}, \\ &M(\mathbf{q})\ddot{\mathbf{q}} + C(\mathbf{q},\dot{\mathbf{q}})\dot{\mathbf{q}} = B(\mathbf{q})\boldsymbol{\tau} + A^T(\mathbf{q})\boldsymbol{\lambda}. \end{aligned} \tag{2}$$

Here, (1) is restated based on the space of admissible velocities, where $\boldsymbol{\eta} \in \mathbb{R}^{\mathfrak{n}-\mathfrak{m}}$ is a vector of quasi-velocities and $N : \mathbb{R}^{\mathfrak{n}} \to \mathbb{R}^{\mathfrak{n}\times(\mathfrak{n}-\mathfrak{m})}$ is the matrix compatible with $\boldsymbol{\eta}$ whose columns span $\ker(A)$, where $\ker(\cdot)$ denotes the kernel of a matrix. We assume existence of such a matrix $\forall \mathbf{q} \in \mathbb{R}^{\mathfrak{n}}$. In the dynamical set of equations, $M : \mathbb{R}^{\mathfrak{n}} \to \mathbb{R}^{\mathfrak{n}\times\mathfrak{n}}$ is the symmetric positive definite mass matrix, $C : \mathbb{R}^{2\mathfrak{n}} \to \mathbb{R}^{\mathfrak{n}\times\mathfrak{n}}$ is the matrix of Coriolis and centrifugal forces, $\boldsymbol{\tau} \in \mathbb{R}^{\mathfrak{s}}$ is the vector of control inputs, and $\boldsymbol{\lambda} \in \mathbb{R}^{\mathfrak{m}}$ is the vector of Lagrange multipliers. The columns of the matrix $B : \mathbb{R}^{\mathfrak{n}} \to \mathbb{R}^{\mathfrak{n}\times\mathfrak{s}}$ are the everywhere linearly independent control directions, and B takes the form $[\mathbb{O}_{\mathfrak{s}\times 3} \ B_2^T(\mathbf{q})]^T$ with $B_2 : \mathbb{R}^{\mathfrak{n}} \to \mathbb{R}^{(\mathfrak{n}-3)\times\mathfrak{s}}$ including the control directions collocated with $\mathbf{q}_2$. Hence,

only direct control over the wheels' rotation and steering angles is assumed.

Assumption 1. We assume that $\mathfrak{s} > \mathfrak{n} - \mathfrak{m}$, and no columns of B are in the image of A^T, i.e., none of the control directions are aligned with the constraint directions.

B. Tractive and Normal Forces

Based on the definition of A, each component of the vector $\boldsymbol{\lambda}$ is the magnitude of the tractive force collocated with the velocity of a wheel-ground contact point specified by the tractive constraint, formed by the corresponding row of A. Note that $\boldsymbol{\lambda}$ only includes the linearly independent constraint forces, and obtaining tractive forces at all wheels based on the nonholonomic model of the rover is infeasible in most applications. Additional information such as a terramechanics model is required to accurately approximate all tractive forces.

Assumption 2. We assume that linearly dependent tractive constraint directions only exist in the lateral direction of the wheels located on the same axle. This assumption is valid for the majority of autonomous rovers/vehicles including car-like and type $(2, 0)$ [35].

The vector $\boldsymbol{\lambda}$ can be determined by differentiating the constraint equations in (1) with respect to time and substituting $\ddot{\mathbf{q}}$ from (2):

$$\begin{aligned} &\mathbb{O}_{\mathfrak{m}\times 1} = \frac{d}{dt}(A\dot{\mathbf{q}}) = A\ddot{\mathbf{q}} + \dot{A}\dot{\mathbf{q}}, \\ &\rightarrow AM^{-1}(-C\dot{\mathbf{q}} + B\boldsymbol{\tau} + A^T\boldsymbol{\lambda}) + \dot{A}\dot{\mathbf{q}} = \mathbb{O}_{\mathfrak{m}\times 1}. \end{aligned} \tag{3}$$

Since the matrix A is full rank and the mass matrix M is everywhere nonsingular, $\boldsymbol{\lambda}$ can be uniquely determined as the function of system's states and control torques by

$$\boldsymbol{\lambda}(\mathbf{q}, \boldsymbol{\eta}, \boldsymbol{\tau}) = V(\mathbf{q}, \boldsymbol{\eta}) + D(\mathbf{q})\boldsymbol{\tau}, \tag{4}$$

where

$$\begin{aligned} V(\mathbf{q}, \boldsymbol{\eta}) &:= -(AM^{-1}A^T)^{-1}(-AM^{-1}C(\mathbf{q}, N\boldsymbol{\eta})N\boldsymbol{\eta} \\ &\quad + \dot{A}(\mathbf{q}, N\boldsymbol{\eta})N\boldsymbol{\eta}) \in \mathbb{R}^{\mathfrak{m}}, \\ D(\mathbf{q}) &:= -(AM^{-1}A^T)^{-1}AM^{-1}B \in \mathbb{R}^{\mathfrak{m}\times\mathfrak{s}}. \end{aligned}$$

Note that the set of kinematical equations in (2) is substituted in these equations.

Let us denote the vector of normal reaction forces at the ground contact points of all wheels by $\mathbf{n} \in \mathbb{R}^{\mathfrak{g}}$.

Assumption 3. We assume that the rover is equipped with individual suspension systems at all wheels and it is always in quasi-static condition in the directions perpendicular to the plane of motion.

Considering the force and moment balance at the rover's chassis and based on Assumption 3, it can be shown that $\mathbf{n}$ is generally formulated as [36]:

$$\mathbf{n} = \mathbf{k} + \Phi(\mathbf{q})\boldsymbol{\lambda} + \Pi(\mathbf{q})\boldsymbol{\tau}, \tag{5}$$

where $\mathbf{k} \in \mathbb{R}^{\mathfrak{g}}$ is a constant vector, and $\Phi\colon \mathbb{R}^{\mathfrak{n}} \rightarrow \mathbb{R}^{\mathfrak{g}\times\mathfrak{m}}$ and $\Pi\colon \mathbb{R}^{\mathfrak{n}} \rightarrow \mathbb{R}^{\mathfrak{g}\times\mathfrak{s}}$ are configuration dependent matrices. These quantities are also dependent on the inertia and geometric parameters of the system, and the gravitational and suspension spring constants. Since the terms included in (5) are dependant on the design of the system, they are discussed in more details in Section IV for a specific autonomous rover system. To simplify our notation at later stages, we define the vector $\mathbf{n}' \in \mathbb{R}^{\mathfrak{m}}$ such that its i^{th} component corresponds to the normal force generating the i^{th} component of $\boldsymbol{\lambda}$. Obviously, this vector includes some repeated elements, since we may consider 2 constraint directions at a wheel associated with a normal force. We relate $\mathbf{n}'$ to the normal reaction forces through the constant matrix $L_n \in \mathbb{R}^{\mathfrak{m}\times\mathfrak{g}}$ such that $\mathbf{n}' = L_n\mathbf{n}$.

C. Output-tracking Control

Let us define $\mathbf{x} := [\mathbf{q}^T, \boldsymbol{\eta}^T]^T \in \mathcal{X} \subset \mathbb{R}^{2\mathfrak{n}}$ as the states of the constrained system. Pre-multiplying both sides of the dynamical equations in (2) by N^T, the reduced state space representation of the system becomes

$$\begin{aligned} \dot{\mathbf{x}} &= \mathbf{f}(\mathbf{x}) + G(\mathbf{x})\boldsymbol{\tau}, \\ \mathbf{f}(\mathbf{x}) &= \begin{bmatrix} N\boldsymbol{\eta} \\ -M_r^{-1}C_r\boldsymbol{\eta} \end{bmatrix}, \quad G(\mathbf{x}) = \begin{bmatrix} \mathbb{O}_{\mathfrak{n}\times\mathfrak{s}} \\ M_r^{-1}B_r \end{bmatrix}, \end{aligned} \tag{6}$$

where $M_r := N^TMN \in \mathbb{R}^{(\mathfrak{n}-\mathfrak{m})\times(\mathfrak{n}-\mathfrak{m})}$, $B_r := N^TB \in \mathbb{R}^{(\mathfrak{n}-\mathfrak{m})\times\mathfrak{s}}$, and $C_r := N^T(M\dot{N}(\mathbf{q}, N\boldsymbol{\eta}) + C(\mathbf{q}, N\boldsymbol{\eta})N) \in \mathbb{R}^{(\mathfrak{n}-\mathfrak{m})\times(\mathfrak{n}-\mathfrak{m})}$ are respectively the reduced mass matrix, the reduced matrix of control directions, and the reduced matrix of Coriolis and centrifugal forces. Let us define $\mathbf{y} \in \mathbb{R}^{\mathfrak{b}}$ as the system's output with the following state functionality:

$$\mathbf{y} = \mathbf{h}(\mathbf{q}), \tag{7}$$

where $\mathbf{h}\colon Q \rightarrow \mathbb{R}^{\mathfrak{b}}$ is assumed to be smooth. Under the assumption that the input-output decoupling matrix

$$F(\mathbf{q}) := \frac{\partial \mathbf{h}}{\partial \mathbf{q}}N(\mathbf{q}) \in \mathbb{R}^{\mathfrak{b}\times(\mathfrak{n}-\mathfrak{m})}, \tag{8}$$

is square, i.e., $\mathfrak{b} = \mathfrak{n} - \mathfrak{m}$, and everywhere nonsingular, the system in (6) is input-output linearizable with relative degree 2, applying the feedback transformation [34]

$$B_r\boldsymbol{\tau} = C_r\boldsymbol{\eta} + M_r(F^{-1}(\mathbf{u} - \mathbf{w})). \tag{9}$$

Here, $\mathbf{u} \in \mathbb{R}^{\mathfrak{b}}$ denotes the control input in the resulting closed loop system, and $\mathbf{w} : \mathcal{X} \rightarrow \mathbb{R}^{\mathfrak{b}}$ is element-wise defined by

$$\mathbf{w}_i := \boldsymbol{\eta}^T N^T \frac{\partial^2 \mathbf{h}_i}{\partial \mathbf{q}^2} N\boldsymbol{\eta} + \sum_{j=1}^{\mathfrak{b}} \left((\frac{\partial \mathbf{h}_i}{\partial \mathbf{q}})^T \frac{\partial N_j}{\partial \mathbf{q}} N\boldsymbol{\eta} \right) \boldsymbol{\eta}_j, \tag{10}$$

for $i = 1 \ldots, \mathfrak{b}$, where N_j denotes the j^{th} column of N, $\boldsymbol{\eta}_j$ is the j^{th} component of $\boldsymbol{\eta}$, and $\mathbf{h}_i$ is the i^{th} component of $\mathbf{h}$. For a comprehensive study of feedback linearizing output functions for rovers, please consult [37]. Let us denote a given twice differentiable desired feasible trajectory for the output by $\mathbf{y}_d(t) \in \mathbb{R}^{\mathfrak{b}}$. The output tracking-error dynamics of the feedback linearized closed loop system becomes:

$$\ddot{\mathbf{y}}_e = \mathbf{v} \in \mathbb{R}^{\mathfrak{b}}, \tag{11}$$

where $\mathbf{y}_e := \mathbf{y} - \mathbf{y}_d$ and $\mathbf{v} := \mathbf{u} - \ddot{\mathbf{y}}_d$. The output-tracking control problem for the system in (6) is defined as finding a control law $\mathbf{v}$ that tracks $\mathbf{y}_d(t)$ with an asymptotically stable

tracking error $\mathbf{y}_e$, such that the tracking error of the internal states remains uniformly bounded. Substituting $\mathbf{u}$ in (9) the output-tracking control law reads:

$$B_r\boldsymbol{\tau} = \mathbf{s}(\mathbf{x}, \mathbf{v}, t), \tag{12}$$

where

$$\mathbf{s}(\mathbf{x}, \mathbf{v}, t) := C_r\boldsymbol{\eta} + M_r(F^{-1}(\mathbf{v} + \ddot{\mathbf{y}}_d - \mathbf{w})) \in \mathbb{R}^{\mathfrak{b}}. \tag{13}$$

Assumption 4. We assume that a rover with the nonholonomic dynamics (2) and output function (7) is static feedback linearizable via the transformation (12); and an asymptotically stabilizing $\mathbf{v}$, e.g., a PID controller, is in place, such that the tracking-error of the internal states is uniformly bounded, for the desired trajectory $\mathbf{y}_d(t)$.

Note that the design and performance of the output-tracking controller is not our concern in this paper, and we refer the readers to [34], for further discussions.

Based on Assumptions 1 and 4, B_r is of rank $\mathfrak{b} < \mathfrak{s}$, indicating that the system contains redundant control directions and (12) has infinite number of solutions when solving for $\boldsymbol{\tau}$. To characterize the space of solutions, let $\boldsymbol{\tau} = \boldsymbol{\tau}_{\parallel} + \boldsymbol{\tau}_{\perp}$ be the decomposition of control actions in the directions of $\ker(B_r)$ and orthogonal to them, such that

$$\boldsymbol{\tau}_{\perp} = W(\mathbf{q})\boldsymbol{\tau}_a \in \ker(B_r). \tag{14}$$

Here, the matrix $W(q) : Q \to \mathbb{R}^{\mathfrak{s}\times(\mathfrak{s}-\mathfrak{b})}$ is defined such that $\mathrm{im}(W) = \ker(B_r)$, and $\boldsymbol{\tau}_a \in \mathbb{R}^{\mathfrak{s}-\mathfrak{b}}$. The image of a matrix is denoted by $\mathrm{im}(\cdot)$. In addition, $\boldsymbol{\tau}_{\parallel}$ is the component of $\boldsymbol{\tau}$ orthogonal to $\ker(B_r)$ and it can be obtained by

$$\boldsymbol{\tau}_{\parallel} = B_r^T(B_rB_r^T)^{-1}\boldsymbol{\tau}_b, \tag{15}$$

for $\boldsymbol{\tau}_b \in \mathbb{R}^{\mathfrak{b}}$. Therefore for an arbitrary $\boldsymbol{\tau}_a$,

$$\boldsymbol{\tau} = \boldsymbol{\tau}_{\parallel} + \boldsymbol{\tau}_{\perp} = B_r^T(B_rB_r^T)^{-1}\mathbf{s} + W\boldsymbol{\tau}_a, \tag{16}$$

is a solution of (12).

Remark 1. The choice of a complementary subspace to $\ker(B_r)$ is not unique. In this paper, the orthogonal subspace to $\ker(B_r)$ in Euclidean sense is considered. If $\boldsymbol{\tau}_a = 0$, the resulting solution for $\boldsymbol{\tau}$ has minimal quadratic norm, referred to as the *uniform control distribution*.

Due to the existence of redundant control directions, an optimal solution minimizing the functional

$$R(\mathbf{x}, \boldsymbol{\tau}, \mathbf{x}_d) = \int_0^{t_f} r(\mathbf{x}, \boldsymbol{\tau}, \mathbf{x}_d)dt, \tag{17}$$

over the system's trajectories can be sought:

$$\min_{\boldsymbol{\tau}_a(\cdot), \boldsymbol{\tau}_b(\cdot)} R(\mathbf{x}, \boldsymbol{\tau}_a, \boldsymbol{\tau}_b, \mathbf{x}_d). \tag{18}$$
$$\text{subject to: (6), (16)}$$

Here, r is a quadratic cost function in $\boldsymbol{\tau}_a$ with positive semi-definite Hessian, t_f is the terminal time, and $\mathbf{x}_d$ is the desired trajectory of the system. As the trajectory of the output is dictated by the control law $\mathbf{v}$ and the desired trajectory $\mathbf{y}_d$, and since the system is not kinematically redundant based on the assumption that $\mathfrak{b} = \mathfrak{n} - \mathfrak{m}$, the constraints in (18) prescribe unique trajectories for $\mathbf{x}_d$, $\mathbf{x}$, and $\boldsymbol{\tau}_b$. Hence, the necessary and sufficient conditions of minimality are obtained in the following simple form [36]:

$$\frac{\partial r}{\partial \boldsymbol{\tau}_a} = \mathbb{O}_{(\mathfrak{s}-\mathfrak{b})\times 1}. \tag{19}$$

A solution of (12) is called the *optimal control distribution*, if $\boldsymbol{\tau}_a$ in (16) satisfies (19) for a cost function r.

The nonholonomic assumption for rovers is valid based on the Coulomb friction model. We introduce the diagonal matrix $\mho \in \mathbb{R}^{\mathfrak{m}\times\mathfrak{m}}$ whose i^{th} diagonal element is the static friction coefficient related to the i^{th} component of $\mathbf{n}'$. In this paper, we assume a box model of the friction cone with independent lateral and longitudinal friction coefficients for each wheel. Once at any wheel-ground contact point the *tractive ratio* passes the static friction threshold in a direction, system experiences dynamic friction (traction loss) and considerable violation of tractive constraints in that direction.

Problem 1 (Dynamic Traction Control). Given the closed loop rover system by (2) and (16) that tracks the (dynamic) trajectory $\mathbf{y}_d(t)$ on a terrain with a specified terrain condition, design a quadratic cost function r such that the optimal control distributions from (19) improve the rover's traction. Traction improvement is defined as reducing the chance of losing traction by distributing the tractive forces $\boldsymbol{\lambda}$ estimated in (4) according to the friction coefficients $\mho$ and approximated normal reaction forces in (5).

III. Traction Optimization

According to the determined functionality of tractive and normal forces under the explained assumptions, a cost function r can be formulated with the aim of improving traction. A seemingly proper choice is the quadratic norm of the vector of tractive ratios weighted by the inverse of static friction coefficients [27]–[31]. Assuming convexity of this cost function, it results in a nonlinear necessary condition of optimality in $\boldsymbol{\tau}_a$, similar to (19). To alleviate this shortcoming, we propose the cost function r to be a quadratic norm of the difference between the tractive forces and their corresponding normal forces scaled by the static friction coefficients. This cost function results in a set of linear necessary and sufficient conditions of optimality in $\boldsymbol{\tau}_a$ and its minimization is directly linked to minimizing the quadratic norm of the tractive ratios. Alignment of the tractive forces with the prescribed rover's motion plays an important role in defining such a cost function.

A. Required Force and Moment

In this section, we define the notion of required force and moment at system's center of mass for a planar rover moving on a prescribed trajectory to introduce reference directions for tractive forces.

Definition 1. The total force and moment that must be generated at the system's center of mass to guarantee tracking of a controlled prescribed trajectory for the output in (7) is called the required force and moment and denoted by $\mathbf{f}_{cm} \in \mathbb{R}^3$.

Based on the assumed state decomposition in Section II-A and the form of matrix B, only tractive forces (not control

torques) directly contribute to the evolution of the total planar momentum of the rover captured by the first three rows of (2). A transformation of these equations is immediately related to the defined notion of required force and moment.

Assumption 5. The system's center of mass is assumed fixed in the main body coordinate frame.

Assumption 5 holds for a large category of rover systems, where steering does not considerably change the location of the center of mass of the steerable wheels and the wheels' yaw moments of inertia are much smaller than that of the main body. Let $\mathbf{y}_c \in \mathbb{R}^3$ be the position and orientation of a coordinate frame attached to the system's center of mass expressed in the inertial frame. Under Assumption 5, it is observed that the velocity of the center of mass is obtained from $\dot{\mathbf{y}}_c = J_c(\theta)\dot{\mathbf{q}}_1$, with the Jacobian $J_c \colon \mathbb{T}^1 \to \mathbb{R}^{3\times 3}$ being invertible and only a function of θ.

Proposition 1. *Based on Assumption 5, the required force and moment expressed in the main body coordinate frame is calculated by:*

$$\mathbf{f}_{cm} = \bar{J}_c M(\dot{N}\boldsymbol{\eta} + NM_r^{-1}(B_r\boldsymbol{\tau}_{\|} - C_r\boldsymbol{\eta})) + \bar{J}_c C\dot{\mathbf{q}}, \quad (20)$$

where the $3 \times \mathfrak{n}$ *matrix*

$$\bar{J}_c = \begin{bmatrix} R_z(\theta)J_c^{-T}(\theta) & \mathbb{O}_{3\times \mathfrak{n}-3} \end{bmatrix} \in \mathbb{R}^{3\times \mathfrak{n}}.$$

Here, $R_z \in \mathbb{R}^{3\times 3}$ *is the in-plane rotation matrix from the inertial coordinate frame to the main body coordinate frame.*

Proof. Under the explained state decomposition in Section II-A, the first three rows of the left hand side of (2) are the time derivative of the total planar momentum of the system about the origin of the main body frame. Based on Assumption 5, pre-multiplying these equations by $R_z J_c^{-T}$ transforms them to the frame attached to the system's center of mass and rotates them to the main body frame. According to the definition of $\bar{J}_c$, this set of equations can be written in the following form:

$$\bar{J}_c M\ddot{\mathbf{q}} + \bar{J}_c C\dot{\mathbf{q}} = \bar{J}_c A^T\boldsymbol{\lambda}. \quad (21)$$

Note that based on the form of matrix B, $\bar{J}_c B = \mathbb{O}_{3\times \mathfrak{s}}$; and hence $\boldsymbol{\tau}$ does not directly appear in the dynamics of the system's center of mass. Now, we substitute $\ddot{\mathbf{q}}$ in (21) by

$$\ddot{\mathbf{q}} = \dot{N}\boldsymbol{\eta} + N\dot{\boldsymbol{\eta}}, \quad (22)$$

derived from the kinematics equations in (2):

$$\bar{J}_c M(\dot{N}\boldsymbol{\eta} + N\dot{\boldsymbol{\eta}}) + \bar{J}_c C\dot{\mathbf{q}} = \bar{J}_c A^T\boldsymbol{\lambda}. \quad (23)$$

In addition, based on (6), we have

$$\dot{\boldsymbol{\eta}} = M_r^{-1}(B_r\boldsymbol{\tau} - C_r\boldsymbol{\eta}). \quad (24)$$

Substituting $\dot{\boldsymbol{\eta}}$ in (23) and considering the decomposition $\boldsymbol{\tau} = \boldsymbol{\tau}_{\|} + \boldsymbol{\tau}_{\perp}$, where $\boldsymbol{\tau}_{\perp} \in \ker(B_r)$,

$$\bar{J}_c M(\dot{N}\boldsymbol{\eta} + NM_r^{-1}(B_r\boldsymbol{\tau}_{\|} - C_r\boldsymbol{\eta})) + \bar{J}_c C\dot{\mathbf{q}} = \bar{J}_c A^T\boldsymbol{\lambda}. \quad (25)$$

The vector on the left hand side of this equation is the required force and moment at the rover's center of mass and expressed in the main body coordinate frame to maintain the system on a controlled prescribed trajectory. □

Corollary 1. *The vector of required force and moment* $\mathbf{f}_{cm}$ *is independent of* $\boldsymbol{\tau}_a$*, and hence the control distribution.*

We define the matrix

$$K := \bar{J}_c A^T \in \mathbb{R}^{3\times \mathfrak{m}}, \quad (26)$$

appearing on the right hand side of (25), whose i^{th} column specifies the contribution of $\boldsymbol{\lambda}_i$ in $\mathbf{f}_{cm}$. This matrix is later used in the detection and accommodation of wheel-fighting.

B. Direction Consideration

An additional shortcoming associated with the conventional traction cost functions proposed in the literature is consideration of the magnitude of tractive forces without including their directions. This may not result in a realistic improvement of a vehicle's traction on various dynamic trajectories. For example, if the magnitude of both lateral and longitudinal tractive forces is considered in traction optimization on a straight line, an unnecessary lateral tractive force distribution will be most likely produced that deteriorates the overall traction of the system. To alleviate this shortcoming, we develop a two-stage optimization algorithm that separately considers the lateral and longitudinal tractive forces with respect to the main body coordinate frame. In the following sections the proposed traction optimization procedure is detailed first for motion on a straight line where system only experiences longitudinal tractive forces, and then for motion on an arbitrary curve. Note that the motion on a straight line or on a curve can be distinguished by measuring the steering angles in autonomous rovers with steering degrees of freedom. In type $(2, 0)$ rovers, estimation of the main body angular velocity can be used to examine whether the system moves on a line or on a curve.

Assumption 6. In what follows, we assume that A is formed in the way that the last $\mathfrak{g} < \mathfrak{m}$ rows capture tractive constraints in the longitudinal directions of all wheels (see Assumption 2) and the rest correspond to the lateral tractive constraints. The directions are specified with respect to the non-spinning local wheel coordinate frames (see Fig.1).

C. Longitudinal Traction Optimization

Based on Assumption 6, let us decompose the vector of magnitudes of tractive forces $\boldsymbol{\lambda}$ as

$$\boldsymbol{\lambda} = \begin{bmatrix} \boldsymbol{\lambda}_l^T & \boldsymbol{\lambda}_f^T \end{bmatrix}^T, \quad (27)$$

where $\boldsymbol{\lambda}_f \in \mathbb{R}^{\mathfrak{g}}$ is called vector of longitudinal tractive forces and $\boldsymbol{\lambda}_l \in \mathbb{R}^{\mathfrak{m}-\mathfrak{g}}$ is coined vector of lateral tractive forces. Accordingly, (4) can be partitioned as:

$$\begin{bmatrix} \boldsymbol{\lambda}_l^T & \boldsymbol{\lambda}_f^T \end{bmatrix}^T = \begin{bmatrix} V_l^T & V_f^T \end{bmatrix}^T + \begin{bmatrix} D_l^T & D_f^T \end{bmatrix}^T \boldsymbol{\tau}, \quad (28)$$

and the matrix K in (26) is structured as $K = [K_l \;\; K_f]$. When the system is moving on a straight line, we consider the following cost function for traction optimization.

$$r_f = \frac{1}{2}(\mho_f \mathbf{n} - \Xi_f\boldsymbol{\lambda}_f)^T(\mho_f \mathbf{n} - \Xi_f\boldsymbol{\lambda}_f), \quad (29)$$

where $\mho_f \in \mathbb{R}^{\mathfrak{g}\times\mathfrak{g}}$ is a diagonal matrix whose elements are the static friction coefficients at each wheel only in longitudinal

direction. Here, $\mathbf{n}$ includes all normal reaction forces, and Ξ_f is the *sign specifier* defined based on the total required longitudinal forces at the system's center of mass:

$$\Xi_f := \begin{cases} 1 & \mathbf{f}_{cm1}(\mathbf{x}, \boldsymbol{\tau}_\parallel) \geq 0, \\ -1 & \mathbf{f}_{cm1}(\mathbf{x}, \boldsymbol{\tau}_\parallel) < 0, \end{cases} \tag{30}$$

where $\mathbf{f}_{cm1}$ is the longitudinal component of $\mathbf{f}_{cm}$.

Remark 2. Note that on a straight line, all wheels are aligned with the rover's motion (only traditional wheels are considered). Hence, Ξ_f provides the reference direction to ensure the alignment of components of tractive forces $\boldsymbol{\lambda}_f$ when performing controlled acceleration or deceleration maneuvers.

Lemma 1. *Based on the normal force approximation in* (5) *and the partitioning in* (28)*, the necessary and sufficient condition of the optimality of the cost function r_f with respect to the control distribution $\boldsymbol{\tau}_a$ is*

$$Q_f^T(\mathbf{p}_f + Q_f \boldsymbol{\tau}_a) = \mathbb{O}_{(\mathfrak{s}-\mathfrak{b})\times 1}, \tag{31}$$

where

$$\mathbf{p}_f := \mho_f(\mathbf{k} + \Phi(V + D\boldsymbol{\tau}_\parallel) + \Pi\boldsymbol{\tau}_\parallel) - \Xi_f(V_f + D_f\boldsymbol{\tau}_\parallel) \in \mathbb{R}^{\mathfrak{g}},$$
$$Q_f := (\mho_f \Phi D + \mho_f \Pi - \Xi_f D_f)W \in \mathbb{R}^{\mathfrak{g}\times(\mathfrak{s}-\mathfrak{b})}.$$

Proof. Substituting $\mathbf{n}$ in (29) from (5),

$$r_f = \frac{1}{2}(\mho_f(\mathbf{k}+\Phi\boldsymbol{\lambda}+\Pi\boldsymbol{\tau}) - \Xi_f\boldsymbol{\lambda}_f)^T(\mho_f(\mathbf{k}+\Phi\boldsymbol{\lambda}+\Pi\boldsymbol{\tau}) - \Xi_f\boldsymbol{\lambda}_f). \tag{32}$$

Then, according to (4) and using the partitioning in (28),

$$r_f = \frac{1}{2}(\mho_f(\mathbf{k} + \Phi(V + D\boldsymbol{\tau}) + \Pi\boldsymbol{\tau}) - \Xi_f(V_f + D_f\boldsymbol{\tau}))^T \\ (\mho_f(\mathbf{k} + \Phi(V + D\boldsymbol{\tau}) + \Pi\boldsymbol{\tau}) - \Xi_f(V_f + D_f\boldsymbol{\tau})). \tag{33}$$

Based on the control decomposition in (16) and the definitions of $\mathbf{p}_f$ and Q_f in the statement of the lemma,

$$r_f = \frac{1}{2}(\mathbf{p}_f + Q_f\boldsymbol{\tau}_a)^T(\mathbf{p}_f + Q_f\boldsymbol{\tau}_a). \tag{34}$$

Note that although the function Ξ_f is discontinuous, the cost function r_f is continuous and differentiable with respect to $\boldsymbol{\tau}_a$. Therefore, (19) leads to the linear necessary and sufficient optimality condition in (31), knowing that the positive semi-definite matrix $Q_f^T Q_f$ is the Hessian. □

Remark 3. Based on Proposition 1, $\mathbf{f}_{cm}$ is independent of the control distribution $\boldsymbol{\tau}_a$; hence, the sign specifier Ξ_f does not change the quadraticity of (34) and accordingly the linearity of (31) with respect to $\boldsymbol{\tau}_a$.

Remark 4. The control directions are throttle/brake and steering torques applied to traditional wheels, a combination of which are dictated by the output tracking controller in (12). Thus, the number of wheels is always greater than or equal to that of redundant control directions, i.e., $\mathfrak{g} \geq (\mathfrak{s} - \mathfrak{b})$.

Since $\mathfrak{g} \geq (\mathfrak{s} - \mathfrak{b})$, the matrix $Q_f^T Q_f \in \mathbb{R}^{(\mathfrak{s}-\mathfrak{b})\times(\mathfrak{s}-\mathfrak{b})}$ is full rank if and only if Q_f is full rank. If the matrix Q_f is well-conditioned, i.e., all of its singular values are greater than a tolerance, the optimal solution $\boldsymbol{\tau}_a^*$ is calculated by

$$\boldsymbol{\tau}_a^* = -(Q_f^T Q_f)^{-1} Q_f^T \mathbf{p}_f. \tag{35}$$

Otherwise, if Q_f is close to rank deficiency, since $Q_f^T\mathbf{p}_f$ is contained in the image of $Q_f^T Q_f$, (31) has infinite number of solutions [38]. To obtain a solution we consider singular value decomposition of $Q_f^T Q_f$, i.e., this matrix is formatted as

$$Q_f^T Q_f = \mathcal{U}\mathcal{S}\mathcal{V}^T, \tag{36}$$

where $\mathcal{U} \in \mathbb{R}^{(\mathfrak{s}-\mathfrak{b})\times(\mathfrak{s}-\mathfrak{b})}$, $\mathcal{V} \in \mathbb{R}^{(\mathfrak{s}-\mathfrak{b})\times(\mathfrak{s}-\mathfrak{b})}$, and $\mathcal{S} \in \mathbb{R}^{(\mathfrak{s}-\mathfrak{b})\times(\mathfrak{s}-\mathfrak{b})}$ is a diagonal matrix whose components are singular values of $Q_f^T Q_f$. Using a tolerance, we identify singular values close to zero. Such singular values in $\mathcal{S}$ and their corresponding columns in $\mathcal{U}$ and $\mathcal{V}$ are then removed and respectively matrices $\mathcal{S}'$, $\mathcal{U}'$, and $\mathcal{V}'$ are formed. Accordingly, a pseudo-inverse solution of $Q_f^T Q_f$ can be determined by $\mathcal{V}'\mathcal{S}'^{-1}\mathcal{U}'^T$ [38], and hence, an optimal solution

$$\boldsymbol{\tau}_a^* = (\mathcal{V}'\mathcal{S}'^{-1}\mathcal{U}'^T)Q_f^T\mathbf{p}_f. \tag{37}$$

D. Wheel-fighting Consideration

Defining traction cost function based on the norm of tractive ratios, may result in the wheel-fighting phenomenon particularly during low-acceleration regimes. In this paper, such phenomenon is defined as follows.

Definition 2. (wheel-fighting) we call a rover's wheel to fight against the rover's motion, if the corresponding tractive force $\boldsymbol{\lambda}_i$ at the wheel has negative contribution in the total required force at system's center of mass $\mathbf{f}_{cm}$, i.e.,

$$\mathbf{f}_{cm}^T K_i \boldsymbol{\lambda}_i < 0, \tag{38}$$

where K_i is the i^{th} column of the matrix K.

To the best of our knowledge, wheel-fighting is not well-studied for the existing dynamic traction controllers in the literature. In this paper, based on the introduced notion of required force and moment at system's center of mass the produced fighting tractive forces are identified and mitigated.

To identify fighting directions, we calculate the longitudinal tractive forces corresponding to the optimal control input $\boldsymbol{\tau}^* := \boldsymbol{\tau}_\parallel + W\boldsymbol{\tau}_a^*$ obtained from (35) or (37) by

$$\boldsymbol{\lambda}_f^* = V_f + D_f\boldsymbol{\tau}^*, \tag{39}$$

and their contributions in the required force $\mathbf{f}_{cm}$ by

$$c_i = \mathbf{f}_{cm}^T K_{fi} \boldsymbol{\lambda}_{fi}^*. \;\; i = 1, \ldots, \mathfrak{g} \tag{40}$$

Here, $\boldsymbol{\lambda}_{fi}^*$ is the i^{th} component of the vector $\boldsymbol{\lambda}_f^*$ and K_{fi} is the i^{th} column of K_f. We collect the fighting longitudinal tractive forces in a vector labelled as $\boldsymbol{\lambda}_{fa} \in \mathbb{R}^{\mathfrak{h}} (\mathfrak{h} < \mathfrak{g})$, based on Definition 2. Accordingly, we form the vector $V_{fa} \in \mathbb{R}^{\mathfrak{h}}$ and the matrix $D_{fa} \in \mathbb{R}^{\mathfrak{h}\times\mathfrak{s}}$ by respectively collecting the rows of V_f and D_f corresponding to the components of $\boldsymbol{\lambda}_{fa}$. To prevent wheel-fighting, we determine a sub-optimal solution obtained by orthogonal projection of the optimal solution to the (affine) subspace of the $\ker(B_r)$ killing such tractive forces. This subspace consists of all $\boldsymbol{\tau}_a \in \mathbb{R}^{\mathfrak{s}-\mathfrak{b}}$ such that $\boldsymbol{\lambda}_{fa} = \mathbb{O}_{\mathfrak{h}\times 1}$, i.e.,

$$V_{fa} + D_{fa}(\boldsymbol{\tau}_\parallel + W\boldsymbol{\tau}_a) = \mathbb{O}_{\mathfrak{h}\times 1}, \\ \rightarrow D_{fa}W\boldsymbol{\tau}_a = -(V_{fa} + D_{fa}\boldsymbol{\tau}_\parallel). \tag{41}$$

If the matrix $D_{fa}W \in \mathbb{R}^{\mathfrak{h}\times(\mathfrak{s}-\mathfrak{b})}$ is full rank with $\mathfrak{h} < (\mathfrak{s}-\mathfrak{b})$, the space of all $\boldsymbol{\tau}_a$ that satisfy (41) can be identified by

$$\boldsymbol{\tau}_a = \boldsymbol{\tau}_{a\|} + W_n \boldsymbol{\tau}_{an}, \tag{42}$$

where

$$\boldsymbol{\tau}_{a\|} = -(D_{fa}W)^T((D_{fa}W)(D_{fa}W)^T)^{-1} (V_{fa} + D_{fa}\boldsymbol{\tau}_{\|}) \in \mathbb{R}^{\mathfrak{s}-\mathfrak{b}} \tag{43}$$

is the right pseudo-inverse solution of (41), $W_n \in \mathbb{R}^{(\mathfrak{s}-\mathfrak{b})\times(\mathfrak{s}-\mathfrak{b}-\mathfrak{h})}$ is a matrix whose columns span $\ker(D_{fa}W)$, i.e., $D_{fa}WW_n = \mathbb{O}_{\mathfrak{h}\times 1}$, and $\boldsymbol{\tau}_{an} \in \mathbb{R}^{(\mathfrak{s}-\mathfrak{b}-\mathfrak{h})}$ is an arbitrary vector. Though if the matrix $D_{fa}W$ is rank deficient, since the vector $-(V_{fa} + D_{fa}\boldsymbol{\tau}_{\|})$ may not be in $\mathrm{im}(D_{fa}W)$, (41) may have no solutions. In this case, the space of closest solutions can be obtained by calculating $\boldsymbol{\tau}_{a\|}$ in (42) using the pseudo inverse solution computed based on singular value decomposition discussed in Section III-C [38].

To alleviate wheel fighting, we orthogonally project the obtained vector of optimal control distribution $\boldsymbol{\tau}_a^*$ from (35) or (37) onto the subspace of solutions of (41). Accordingly, the sub-optimal solution $\boldsymbol{\tau}_a^{*'}$ is obtained by

$$\boldsymbol{\tau}_a^{*'} = \boldsymbol{\tau}_{a\|} + W_n \boldsymbol{\tau}_{an\|}, \tag{44}$$

where $\boldsymbol{\tau}_{a\|}$ is calculated from (43), and

$$\boldsymbol{\tau}_{an\|} = (W_n^T W_n)^{-1} W_n^T (\boldsymbol{\tau}_a^* - \boldsymbol{\tau}_{a\|}) \tag{45}$$

is the left pseudo-inverse solution. Note that since W_n is a full column matrix, $W_n^T W_n$ is always invertible.

Remark 5. The solution $\boldsymbol{\tau}_a^{*'}$ is not optimizing the defined cost function r_f, but since the orthogonal projection is used, it is the closest solution to $\boldsymbol{\tau}_a^*$ in the space of control distributions alleviating the fighting tractive forces. The optimality of $\boldsymbol{\tau}_a^{*'}$ can be investigated applying Karush–Kuhn–Tucker theorem which is out of scope of this paper [39].

Remark 6. If the dimension of $\boldsymbol{\lambda}_{fa}$ is greater than or equal to that of $\boldsymbol{\tau}_a$, i.e. $\mathfrak{h} \geq \mathfrak{s}-\mathfrak{b}$, the optimization becomes over-constrained, and the pseudo inverse solution provides the best control distribution, i.e., $\boldsymbol{\tau}_a^* = 0$.

Since we may introduce new fighting directions when applying $\boldsymbol{\tau}_a^{*'}$, the detailed algorithm in this section can be repeated for the sub-optimal control distribution $\boldsymbol{\tau}_a^{*'}$. In this process, we shrink the space of sub-optimal solutions by adding new constraints, until we find a solution or exit without obtaining a distribution. In the latter case, $\boldsymbol{\tau}_a = 0$ provides the best control distribution. The complete flowchart of the longitudinal traction optimization algorithm is depicted in Fig.2.

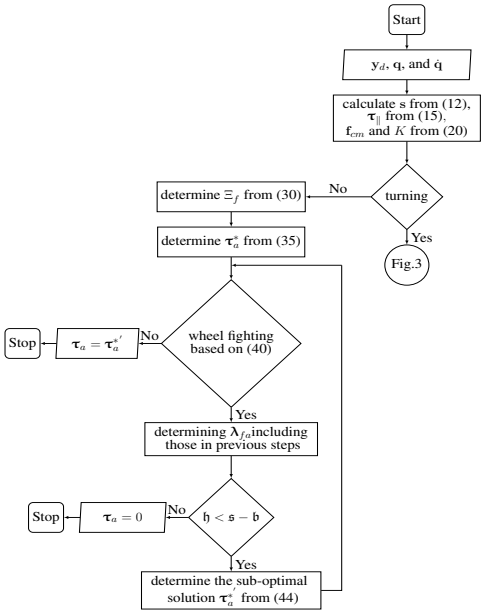

Fig. 2: Flowchart of the longitudinal traction optimization

E. Lateral and Longitudinal Traction Optimization

In this paper, we propose a two-stage optimization algorithm for traction improvement when the system is tracking a trajectory with nonzero curvature. In the first stage, we focus on the traction improvement in the lateral direction of the main body coordinate frame. Often, this negatively impacts the traction in the longitudinal direction due to generating a moment about system's center of mass, which will be minimized as part of the objective function proposed for the first stage of optimization. The rover's traction in the longitudinal direction of the wheels is then optimized separately in the second stage.

1) Lateral Traction Optimization: Under Assumption 6, the vectors $\boldsymbol{\lambda}_l \in \mathbb{R}^{\mathfrak{k}}$ $(\mathfrak{k} = \mathfrak{m}-\mathfrak{g})$ and $\boldsymbol{\lambda}_f \in \mathbb{R}^{\mathfrak{g}}$ respectively contain the magnitude of tractive forces in the lateral and longitudinal directions of the wheels' local frames. Considering the orientation of the local frames (steering angles), we form the vectors $\boldsymbol{\lambda}_{lb} \in \mathbb{R}^{\mathfrak{k}}$ and $\boldsymbol{\lambda}_{fb} \in \mathbb{R}^{\mathfrak{g}}$ whose components are respectively the lateral and longitudinal tractive forces in the main body frame. The application of these forces are at the wheel-ground contact points specified by the rows of the matrix A. The functionality of $\boldsymbol{\lambda}_{lb}$ and $\boldsymbol{\lambda}_{fb}$ is specified by $\boldsymbol{\lambda}_{lb} = \Upsilon_l(\mathbf{q})\boldsymbol{\lambda}$ and $\boldsymbol{\lambda}_{fb} = \Upsilon_f(\mathbf{q})\boldsymbol{\lambda}$, where the full-rank matrices $\Upsilon_l \in \mathbb{R}^{\mathfrak{k}\times\mathfrak{m}}$ and $\Upsilon_l \in \mathbb{R}^{\mathfrak{g}\times\mathfrak{m}}$ form an invertible transformation $\Upsilon(\mathbf{q}) \in \mathbb{R}^{\mathfrak{m}\times\mathfrak{m}}$, such that

$$\boldsymbol{\lambda}_b := \begin{bmatrix}\boldsymbol{\lambda}_{lb}\\ \boldsymbol{\lambda}_{fb}\end{bmatrix} = \begin{bmatrix}\Upsilon_l\\ \Upsilon_f\end{bmatrix}\boldsymbol{\lambda} =: \Upsilon\boldsymbol{\lambda}.$$

The existence of such transformations is assumed under the nominal operating conditions of the rover. This implies that the constraint equations can be rewritten as $\Upsilon^T A\dot{\mathbf{q}} = \mathbb{O}_{\mathfrak{m}\times 1}$, while $\boldsymbol{\lambda}_b$ acts as the vector of Lagrange multipliers. Based on these transformations, we also define the matrix of static friction coefficients in the lateral and longitudinal direction of the main body $\mho_l := \Upsilon_l(\mathbf{q})\mho$ and $\mho_f := \Upsilon_f(\mathbf{q})\mho$, respectively.

The lateral traction optimization problem can be stated as obtaining an optimal distribution of the components of $\boldsymbol{\lambda}_{lb}$ on a prescribed trajectory, considering the scaled normal forces by static friction coefficients in the main body's lateral direction, summarized in $\mho_l\mathbf{n}^{'}$. This distribution often generates an excess moment about system's center of mass in comparison to the required moment $\mathbf{f}_{cm3}$, the third component of $\mathbf{f}_{cm}$. This excess moment must be compensated by longitudinal tractive forces. In other words, traction improvement in lateral direction negatively impacts traction in the longitudinal di-

rection. Hence, the difference between the generated moment at system's center of mass by components of $\boldsymbol{\lambda}_{lb}$ and $\mathbf{f}_{cm3}$, weighted by a positive constant υ, must be included in the the cost function for traction optimization. Let $\Upsilon_t \colon \mathbb{R}^{\mathfrak{k}} \to \mathbb{R}$ denote the the constant row vector mapping $\boldsymbol{\lambda}_{lb}$ to the torque it generates at system's center of mass, namely m_{lb}, i.e.,

$$m_{lb} = \Upsilon_t \Upsilon_l(\mathbf{q})\boldsymbol{\lambda}. \tag{46}$$

We then define the cost function r_l for lateral traction optimization as:

$$r_l = (\Gamma\mathbf{n} - \Upsilon\boldsymbol{\lambda} - \boldsymbol{\kappa})^T \Lambda (\Gamma\mathbf{n} - \Upsilon\boldsymbol{\lambda} - \boldsymbol{\kappa}), \tag{47}$$

where

$$\Gamma := \begin{bmatrix} \mho_l L_n \\ \mathbb{O}_{1\times\mathfrak{g}} \end{bmatrix} \in \mathbb{R}^{(\mathfrak{k}+1)\times\mathfrak{g}},\ \Upsilon := \begin{bmatrix} \Xi_l \Upsilon_l(\mathbf{q}) \\ -\Upsilon_t \Upsilon_l(\mathbf{q}) \end{bmatrix} \in \mathbb{R}^{(\mathfrak{k}+1)\times\mathfrak{m}},$$
$$\boldsymbol{\kappa} := \begin{bmatrix} \mathbb{O}_{\mathfrak{k}\times 1} \\ \mathbf{f}_{cm3}(\mathbf{x}, \boldsymbol{\tau}_{\|}) \end{bmatrix} \in \mathbb{R}^{\mathfrak{k}+1},\ \Lambda := \begin{bmatrix} \mathbb{I}_{\mathfrak{k}\times\mathfrak{k}} & \mathbb{O}_{\mathfrak{k}\times 1} \\ \mathbb{O}_{1\times\mathfrak{k}} & \upsilon \end{bmatrix} \in \mathbb{R}^{(\mathfrak{k}+1)\times(\mathfrak{k}+1)}. \tag{48}$$

Here, Ξ_l is the sign specifier for the total required lateral force at the system's center of mass:

$$\Xi_l = \begin{cases} 1 & \mathbf{f}_{cm2}(\mathbf{x}, \boldsymbol{\tau}_{\|}) \geq 0 \\ -1 & \mathbf{f}_{cm2}(\mathbf{x}, \boldsymbol{\tau}_{\|}) < 0 \end{cases} \tag{49}$$

where $\mathbf{f}_{cm2}$ is the second component of $\mathbf{f}_{cm}$.

Remark 7. Since determination of the terms Υ_l, L_n, and Υ_t is dependant on the structure and the type of the autonomous rover/vehicle, it is discussed in more detail in section IV for a specific autonomous rover system.

Lemma 2. *Based on the tractive and normal force approximations in* (4) *and* (5)*, respectively, the necessary condition of the optimality of the cost function r_l with respect to the control distribution $\boldsymbol{\tau}_a$ is*

$$Q_l^T \Lambda Q_l \boldsymbol{\tau}_a = -Q_l^T \Lambda \mathbf{p}_l, \tag{50}$$

where

$$\mathbf{p}_l := \Gamma(\mathbf{k} + \Phi(V + D\boldsymbol{\tau}_{\|}) + \Pi\boldsymbol{\tau}_{\|}) - \Upsilon(V + D\boldsymbol{\tau}_{\|}) - \boldsymbol{\kappa} \in \mathbb{R}^{\mathfrak{k}+1},$$
$$Q_l := (\Gamma\Phi D + \Gamma\Pi - \Upsilon D)W \in \mathbb{R}^{(\mathfrak{k}+1)\times(\mathfrak{s}-\mathfrak{b})}. \tag{51}$$

Proof. Substituting $\mathbf{n}$ in (47) by (5), r_l becomes

$$r_l = (\Gamma(\mathbf{k}+\Phi\boldsymbol{\lambda}+\Pi\boldsymbol{\tau}) - \Upsilon\boldsymbol{\lambda} - \boldsymbol{\kappa})^T \Lambda (\Gamma(\mathbf{k}+\Phi\boldsymbol{\lambda}+\Pi\boldsymbol{\tau}) - \Upsilon\boldsymbol{\lambda} - \boldsymbol{\kappa}). \tag{52}$$

From (4), we can also substitute $\boldsymbol{\lambda}$ in (52):

$$r_l = (\Gamma(\mathbf{k} + \Phi(V + D\boldsymbol{\tau}) + \Pi\boldsymbol{\tau}) - \Upsilon(V + D\boldsymbol{\tau}) - \boldsymbol{\kappa})^T \Lambda (\Gamma(\mathbf{k} + \Phi(V + D\boldsymbol{\tau}) + \Pi\boldsymbol{\tau}) - \Upsilon(V + D\boldsymbol{\tau}) - \boldsymbol{\kappa}). \tag{53}$$

Considering the decomposition of $\boldsymbol{\tau}$ in (16) and introducing $\mathbf{p}_l$ and Q_l as defined in the statement of lemma, (52) becomes

$$\frac{1}{2}(\mathbf{p}_l + Q_l\boldsymbol{\tau}_a)^T \Lambda (\mathbf{p}_l + Q_l\boldsymbol{\tau}_a). \tag{54}$$

Note that although the function Ξ_l is discontinuous, the cost function r_l is continuous and differentiable in $\boldsymbol{\tau}_a$. Hence, (19) leads to the linear necessary and sufficient optimality condition in (50), given that the positive semi-definite matrix $Q_l^T \Lambda Q_l$ is the Hessian. □

Assumption 7. We assume that the dimension of the vector $\boldsymbol{\lambda}_{lb}$ is less than the number of redundant control directions, i.e. $\mathfrak{k} < \mathfrak{s} - \mathfrak{b}$.

Based on Assumption 7, the matrix $Q_l^T \Lambda Q_l$ is not full-rank. Accordingly, since $Q_l^T \Lambda \mathbf{p}_l$ is contained in the $\text{im}(Q_l^T \Lambda Q_l)$, (50) has infinite number of solutions, in the following form:

$$\boldsymbol{\tau}_{a1}^* = \boldsymbol{\tau}_{l\|}^* + Q_{ln}^{'} \boldsymbol{\tau}_{ln}, \tag{55}$$

where $Q_{ln}^{'}$ denotes a matrix whose columns span the $\ker(Q_l^T \Lambda Q_l)$ and $\boldsymbol{\tau}_{ln}$ is an arbitrary vector. The unique vector $\boldsymbol{\tau}_{l\|}^*$ in the subspace orthogonal to the $\ker(Q_l^T \Lambda Q_l)$ can be obtained applying the pseudo inverse solution computed using singular value decomposition studied in Section III-C.

2) Longitudinal Traction Optimization: The second stage of traction control involves traction optimization in the longitudinal direction of the main body, within the space of optimal solutions obtained in (55). Similar to (29), this optimization is formulated as finding the optimal vector $\boldsymbol{\tau}_{ln}$ that minimizes the following cost function:

$$r_{fl} = \frac{1}{2}(\Gamma_f \mathbf{n} - \Xi_{fl} \Upsilon_f \boldsymbol{\lambda})^T (\Gamma_f \mathbf{n} - \Xi_{fl} \Upsilon_f \boldsymbol{\lambda}), \tag{56}$$

where $\Gamma_f = \mho_f L_n \in \mathbb{R}^{\mathfrak{g}\times\mathfrak{g}}$ and $\Xi_{fl} \in \mathbb{R}^{\mathfrak{g}\times\mathfrak{g}}$ it a diagonal matrix whose components are the sign specifier for the elements of $\boldsymbol{\lambda}_{fb}$. Since r_{fl} is optimized within the space of solutions obtained in (55), the sign specifier Ξ_{fl} must be defined considering the contribution of the first stage of optimization. We decompose the vector of required force and moment $\mathbf{f}_{cm}$ that is independent of the control distribution into two components: (i) the contribution of the lateral tractive forces $\mathbf{f}_{cml}$, and (ii) the contribution of the longitudinal tractive forces $\mathbf{f}_{cmf}$. That is,

$$\mathbf{f}_{cm} = \mathbf{f}_{cml} + \mathbf{f}_{cmf} = K\boldsymbol{\lambda} = K\Upsilon^{-1}\boldsymbol{\lambda}_b =: \begin{bmatrix} K_{lb} & K_{fb} \end{bmatrix} \begin{bmatrix} \boldsymbol{\lambda}_{lb} \\ \boldsymbol{\lambda}_{fb} \end{bmatrix}, \tag{57}$$

where the matrices $K_{lb} \in \mathbb{R}^{3\times\mathfrak{k}}$ and $K_{fb} \in \mathbb{R}^{3\times\mathfrak{g}}$ evaluate the contributions $\mathbf{f}_{cml} = K_{lb}\boldsymbol{\lambda}_{lb}$ and $\mathbf{f}_{cmf} = K_{fb}\boldsymbol{\lambda}_{fb}$. For any optimal vector $\boldsymbol{\lambda}_{lb}^*$ from the first stage of optimization, we can then determine the components of the sign specifier Ξ_{fl} based on the vector $\mathbf{f}_{cmf} = \mathbf{f}_{cm} - K_{lb}\boldsymbol{\lambda}_{lb}^*$.

Remark 8. Properly defining the sign specifier Ξ_{fl} using $\mathbf{f}_{cmf}$ is a nontrivial task for rover systems with complex geometries, since both longitudinal and rotational directions at the center of mass must be considered. For the vehicles with wheels located on the port and starboard sides that are equally laterally distanced (for example, car-like rovers), the lumped longitudinal forces at both sides, respectively denoted by λ_{flp} and λ_{fls}, are considered. Then, based on the first and last components of $\mathbf{f}_{cmf}$, these lumped forces can be obtained by solving a system of two linear equations with two unknowns. We specify the component of Ξ_{fl} for each wheel equal to the sign of the lumped tractive force at its corresponding side. That is, for the i^{th} wheel on the port or starboard side we respectively have

$$\Xi_{fli} = \begin{cases} +1 & \lambda_{flp} \geq 0 \\ -1 & \lambda_{flp} < 0 \end{cases} \quad \text{or} \quad \Xi_{fli} = \begin{cases} +1 & \lambda_{fls} \geq 0 \\ -1 & \lambda_{fls} < 0 \end{cases}$$

Note that the optimal solution $\boldsymbol{\lambda}_{lb}^{*}$ and hence Ξ_{fl} is not necessarily independent of $\boldsymbol{\tau}_{ln}$.

Assumption 8. We assume that the arbitrary choice of the vector $\boldsymbol{\tau}_{ln}$ in the second stage of optimization does not affect the vector $\mathbf{f}_{cmf}$ in a fashion that leads to a sign change in the components of Ξ_{fl}.

Similar to the case of traction optimization only in the longitudinal direction, substituting $\mathbf{n}$ and $\boldsymbol{\lambda}$ from (5) and (4), respectively, and considering the space of solutions in (55) we introduce

$$\begin{aligned}\mathbf{p}_{fl} :=&\Gamma_f(\mathbf{k}+\Phi(V+D\boldsymbol{\tau}_{\|}+DW\boldsymbol{\tau}_{l\|}^{*})+\Pi(\boldsymbol{\tau}_{\|}+W\boldsymbol{\tau}_{l\|}^{*}))\\ &-\Xi_{fl}\Upsilon_f(V+D\boldsymbol{\tau}_{\|}+DW\boldsymbol{\tau}_{l\|}^{*}),\\ Q_{fl} :=&(\Gamma_f\Phi D+\Gamma_f\Pi-\Xi_{fl}\Upsilon_f D)WQ_{ln}^{'},\end{aligned}$$

which convert the r_{fl} into

$$r_{fl}=\frac{1}{2}(\mathbf{p}_{fl}+Q_{fl}\boldsymbol{\tau}_{ln})^{T}(\mathbf{p}_{fl}+Q_{fl}\boldsymbol{\tau}_{ln}). \tag{58}$$

Then following the same lines of proof as in Lemma 1, the necessary condition for the optimal solution $\boldsymbol{\tau}_{ln}^{*}$ becomes

$$Q_{fl}^{T}Q_{fl}\boldsymbol{\tau}_{ln}=-Q_{fl}^{T}\mathbf{p}_{fl}. \tag{59}$$

If the matrix $Q_{fl}^{T}Q_{fl}$ is well-conditioned, the optimal solution $\boldsymbol{\tau}_{ln}^{*}$ can be uniquely determined as

$$\boldsymbol{\tau}_{ln}^{*}=-(Q_{fl}^{T}Q_{fl})^{-1}Q_{fl}^{T}\mathbf{p}_{fl}. \tag{60}$$

However, if the matrix $Q_{fl}^{T}Q_{fl}$ is close to rank deficiency the singular value decomposition approach discussed in Section III-C is implemented.

The procedure for preventing wheel fighting as detailed in Section III-D is implemented for the resultant vector $\boldsymbol{\lambda}_f$. The only difference here is that only the first and last components of the vector $\mathbf{f}_{cmf}$ are considered during examining the contributions, since the second component is related to the first stage of optimization. The complete flowchart of the traction optimization algorithm on trajectories with nonzero curvature is depicted in Fig.3.

Remark 9. Since $\mathfrak{k}$ is often small, introducing wheel fighting in the lateral direction after the first optimization is less probable. However, we can test the contribution of generated lateral forces in the required lateral force and if the system experiences wheel fighting, only the pseudo inverse solution is used. The same procedure applies whenever the number of tractive forces that must be killed is more than or equal to the dimension of $\boldsymbol{\tau}_{ln}$ in the second stage of optimization.

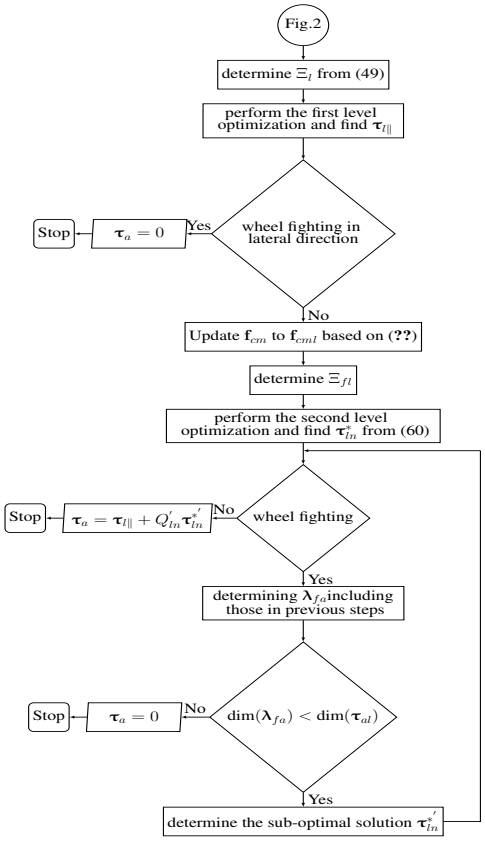

Fig. 3: Lateral and longitudinal traction optimization

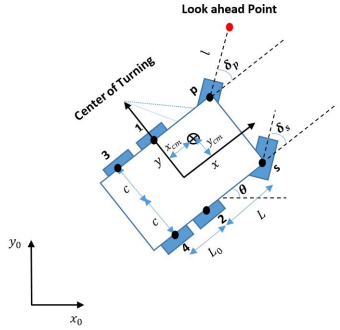

Fig. 4: Schematic of the system

IV. Implementation on a Six-wheel Lunar Rover

The proposed dynamic traction controller is implemented on a six-wheel type $(1,1)$ autonomous Lunar rover, modelled as the composition of a main body and six driven wheels located on three parallel axles (front, center, and rear). Only the front wheels are steerable, whose steering angles δ_p (port side) and δ_s (starboard side) satisfy the Ackerman condition. The schematic of the system is depicted in Fig. 4, where x_0y_0-frame is the inertial frame, xy-frame is the body-fixed frame located at the middle of the center axle, and some geometrical parameters are specified. The elements of the 10-dimensional configuration space of the system are denoted by $\mathbf{q} = [x_b\ y_b\ \theta\ \psi_s\ \psi_1\ \psi_2\ \psi_3\ \psi_4\ \psi_p\ \delta_p]^T$. Here, $\mathbf{q}_1 = [x_b\ y_b\ \theta]^T \in \mathbb{R}^3$ is the position and orientation of xy-frame from x_0y_0-frame, $\psi_s, \psi_p \in \mathbb{R}$ are respectively the rotation of the starboard and port front wheels, and $\psi_1, \psi_2, \psi_3, \psi_4, \in \mathbb{R}$ refer to the rotation of port center, starboard center, port rear, and starboard rear wheel, respectively.

The imposed tractive constraints are in the form of no longitudinal and lateral slip conditions at all wheels, except for rear wheels, where no-lateral velocity constraint is relaxed (mobility consideration). The number of everywhere linearly independent tractive constraints is $\mathfrak{m} = 8$. We form the constraint matrix $A \in \mathbb{R}^{8\times 10}$ whose first and second rows

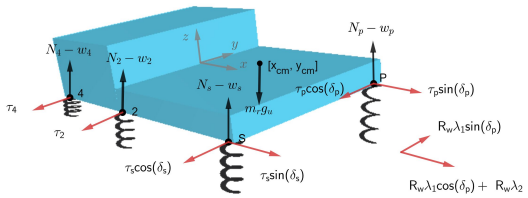

Fig. 5: Free-body diagram of the main body

refer to the no-lateral velocity constraints at the port front wheel and the center wheels, respectively. The remaining rows correspond to the no-longitudinal velocity constraints at all six wheels. Note that the no-lateral velocity constraints at starboard wheels are linearly dependent on those at port wheels (front and center). The vector of control inputs $\boldsymbol{\tau}$ consists of applied driving torques at all wheels and the steering torque at port front wheel, i.e., $\mathfrak{s} = 7$, and the matrix of control directions $B = [\mathbb{O}_{7\times 3} \;\; \mathbb{I}_{7\times 7}]^T$. We choose the 2-dimensional quasi-velocity vector $\boldsymbol{\eta} = \begin{bmatrix}\dot{\psi}_p & \dot{\delta}_p\end{bmatrix}^T$. The stabilizing control law $\mathbf{v}$ in (11) is selected as a PID law whose gains are shown in Table I. The explicit equation for A can be found in [34, Eq. 75], and the details of the dynamic model and input-output linearization of the rover are presented in [34, Section V].

Under Assumption 3, we approximate normal reaction forces based on the free-body diagram of the main body in Fig. 5, where forces and moments are illustrated by black and red arrows, respectively. Note that N_i and w_i, for $i = 1, \ldots, 6$, are respectively the normal forces at the wheels and wheel weights, which are assumed equal to the constant $w_w = m_w g_u$ (see Table I). According to Assumption 3, the summation of all forces in the vertical direction is equal to zero, i.e.,

$$N_1 + N_2 + N_3 + N_4 + N_p + N_s - m_r g_u - 6w_w = 0, \quad (61)$$

Additionally, we have

$$\begin{aligned} +\curvearrowleft \sum M_{p4} &= (N_1 + N_2)L_0 + (N_p + N_s)(L_0 + L) \\ -(x_{cm} + L_0)m_r g_u &- 2w_w(2L_0 + L) + R_w \boldsymbol{\phi}_1^T \boldsymbol{\lambda} + \boldsymbol{\pi}_1^T \boldsymbol{\tau} = 0, \\ +\curvearrowleft \sum M_{r4} &= (N_1 + N_3 + N_p)2c - (y_{cm} + c)m_r g_u \\ &-6w_w c + R_w \boldsymbol{\phi}_2^T \boldsymbol{\lambda} + \boldsymbol{\pi}_2^T \boldsymbol{\tau} = 0, \end{aligned}$$

where $\sum M_{r4}$ and $\sum M_{p4}$ are the total moment about Point 4 in x- and y-direction of the main body, respectively, and

$$\begin{aligned} &\boldsymbol{\phi}_1 = \begin{bmatrix}-\sin(\delta_p) & \mathbb{O}_{1\times 7}\end{bmatrix}^T, \quad \boldsymbol{\phi}_2 = \begin{bmatrix}\cos(\delta_p) & 1 & \mathbb{O}_{1\times 6}\end{bmatrix}^T, \\ &\boldsymbol{\pi}_1 = \begin{bmatrix}\cos(\delta_s) & 1 & 1 & 1 & 1 & \cos(\delta_p) & 0\end{bmatrix}^T, \\ &\boldsymbol{\pi}_2 = \begin{bmatrix}\sin(\delta_s) & \mathbb{O}_{1\times 4} & \sin(\delta_p) & 0\end{bmatrix}^T. \end{aligned}$$

To determine all normal forces, we assume vertical force transfer to a rigid main body through suspension springs:

$$\begin{aligned} &\Delta_2 = \Delta_4 - L_0\Delta_{pi}, \quad \Delta_s = \Delta_4 - (L + L_0)\Delta_{pi}, \\ &\Delta_3 = \Delta_4 - (2c)\Delta_{ro}, \quad \Delta_1 = \Delta_4 - L_0\Delta_{pi} - 2c\Delta_{ro}, \\ &\Delta_p = \Delta_4 - (L + L_0)\Delta_{pi} - 2c\Delta_{ro}, \end{aligned} \quad (62)$$

where Δ_1, Δ_2, Δ_3, and Δ_4 are respectively the deformation of the springs at the wheels $1, 2, 3$, and 4 (see Fig.5), Δ_s and Δ_p are the spring deformations at the starboard and port front wheels, respectively, and the roll angle Δ_{ro} and pitch angle Δ_{pi} are assumed small. The spring constants are denoted by k_f 9front wheels), k_c (center wheels), and k_r (rear wheels). Considering this set of equations and the Hook's law, we obtain 6 linearly independent equations to uniquely determine the terms Φ, Π, and $\mathbf{k}$ in (5), and hence $\mathbf{n}$ (Appendix A). In Appendix A, we also report L_n, where for the wheels with linearly dependent constraints, average of the normal forces at involved wheels is considered. Further, details of calculating $\mathbf{f}_{cm}$ and K based on (20) and (26) are discussed in [36].

The matrix Υ_l and the row vector Υ_t in (48) are formed as

$$\begin{aligned} \Upsilon_l &= \begin{bmatrix}\cos(\delta_p) & 0 & \sin(\delta_p) & \sin(\delta_s) & 0 & 0 & 0 & 0 \\ 0 & 1 & 0 & 0 & 0 & 0 & 0 & 0\end{bmatrix}, \\ \Upsilon_t &= \begin{bmatrix}(L - x_{cmt}) & -x_{cmt} & (L - x_{cmt}) & (L - x_{cmt}) & \mathbb{O}_{1\times 4}\end{bmatrix}. \end{aligned}$$

The first row of matrix Υ_l captures the contribution of the longitudinal and lateral tractive forces at front wheels in the lateral direction of motion. Similarly, matrix Υ_f is obtained:

$$\Upsilon_f = \begin{bmatrix}-\sin(\delta_p) & 0 & 1 & 0 & \mathbb{O}_{1\times 4} \\ 0 & 0 & 0 & 1 & \mathbb{O}_{1\times 4} \\ \mathbb{O}_{4\times 1} & \mathbb{O}_{4\times 1} & \mathbb{O}_{4\times 1} & \mathbb{O}_{4\times 1} & \mathbb{I}_{4\times 4}\end{bmatrix}. \quad (63)$$

Considering the lumped longitudinal tractive force in the main body frame at port side λ_{flp} and starboard side λ_{fls}, the set of two linear equations used in determination of Ξ_{fl} becomes

$$\lambda_{flp} + \lambda_{fls} = \mathbf{f}_{cmf1}, \quad \lambda_{flp} - \lambda_{fls} = \mathbf{f}_{cmf3}/c. \quad (64)$$

A. *Software-in-the-loop simulation results*

The proposed traction controller is evaluated in a software-in-the-loop simulation. We code the controller in MATLAB and use a digital twin of the rover modeled in Vortex Studio (see Fig.6). Vortex Studio is a high-fidelity multi-body dynamics simulator equipped with various wheel-ground interaction models, developed by CM Labs Simulation Inc. [40], [41]. The

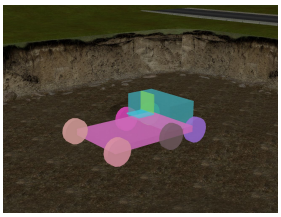

Fig. 6: The designed mechanism in Vortex

values of kinematic, dynamic and control parameters used in the model are depicted in Table I. The suspension system also consists of dampers with coefficients 10KNs/m, 15KNs/m, and 20KNs/m for front, center and rear wheels, respectively. Wheel-ground interaction is modelled based on the box model of dry friction cone, where lateral and longitudinal friction coefficients are independent.

The desired trajectory of the system is moving on a straight line for 30s with a forward velocity profile of $0.4t \sin\left(\frac{4\pi}{30}\right)^2$m/s. Rover is then accelerates with 0.3m/s^2 for 8 s and continues its motion with a constant forward velocity until 55^{th} second. At 40^{th} second a fast steering command is applied and system starts circling. At 55^{th} second we apply

Rover Parameters			
L[m]	L_0[m]	c[m]	R_w[m]
1	0.5	0.55	0.2
l[m]	x_{cm}[m]	y_{cm}[m]	m_r[Kg]
1	-0.0667	0	600
m_w[Kg]	J_r[Kg/m^2]	J_{wy}[Kg/m^2]	J_{wz}[Kg/m^2]
40	450	1	1
g_u[m/s^2]	k_f[N/m]	k_c[N/m]	k_r[m/s]
1.632	30000	45000	60000
Controller Gains			
K_p	K_I	K_d	
48	64	12	

TABLE I: Lunar rover's model and controller parameters.

a brake command with -0.05m/s^2 for 5s. After circling with the reduced constant velocity for another 5s, we apply another acceleration command of 0.05m/s^2 for 20s. Then system continues with constant velocity. Fig.7 depicts this trajectory that is designed to evaluate the efficacy of the traction controller while the system undergoes various maneuvers at the verge of traction loss in both longitudinal and lateral directions.

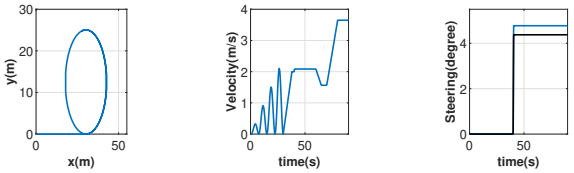

(a) (b) (c)

Fig. 7: Desired trajectory: (a) desired path (b) desired forward velocity profile (c) desired steering angles.

We ran the simulation once with the conventional pseudo-inverse solution, denoted by "Pinv", and once with the optimal control distribution, denoted by "Optimal". Fig. 8 compares the Root Mean Square (RMS) of the tractive ratios at all wheels in both longitudinal and lateral directions. It is observed that during linear motion with low accelerations due to the definition of the proposed cost function and wheel-fighting mitigation strategy, optimal distribution does not considerably impact the overall traction. During deceleration phases since the normal forces at different axles are comparable, the optimal approach produces tractive ratios close to those in the Pinv case. However the tractive ratios are considerably improved in the Optimal approach during high acceleration phases, where the system is closer to the verge of traction loss. Particularly, the dynamic traction controller saves the system from drifting at 24^{th} second, evident from the sudden drop in the RMS of tractive rations in the Pinv case. During circling, clearly

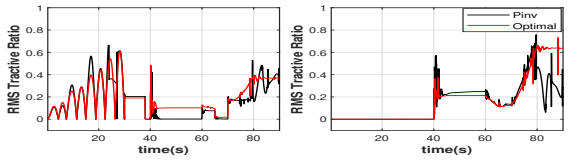

(a) (b)

Fig. 8: RMS of Tractive ratios (a) longitudinal, (b) lateral.

the proposed optimal control distribution improves the tractive ratios in the lateral direction at the expense of increasing tractive ratios in the longitudinal direction. In comparison to the Pinv case, the Optimal approach saves the system from traction loss in the lateral direction in two incidents: (i) when the sharp steering command is applied ($t = 40$s), and (ii) when the system circles with a high velocity ($t = 80$s). Fig. 9 compares the output tracking errors observed by the controller in both Optimal and Pinv cases, demonstrating a close match, except when the system experiences traction loss.

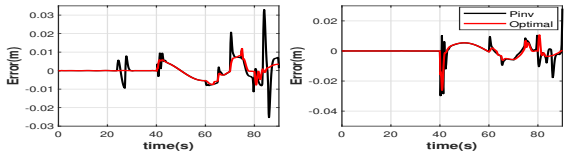

(a) (b)

Fig. 9: Comparison of the ooutpu error in: (a) x, (b) y direction

V. CONCLUSION

In the next-generation space missions, autonomous rovers must reliably perform dynamic maneuvers with high velocities and accelerations. In this paper, we proposed a traction control strategy that can ensure safe traverse of such systems on rough firm terrains. We developed this strategy to be fast and practical by designing novel cost functions requiring minimal information about wheel-ground interaction models and resulting in linear optimality conditions. For the first time, we considered both longitudinal and lateral tractive optimization on dynamic prescribed trajectories of the system. A software-in-the-loop simulation environment equipped with realistic wheel-ground interaction and tire models was developed. In this simulator, we implemented the proposed dynamic traction controller on a six-wheel autonomous Lunar rover and exhaustively tested it. The simulation results demonstrated meaningful improvement in the traction of the rovers with dynamic motions. The traction control strategy was able to save the system from traction loss in multiple occasions. The future directions of this work include consideration of actuators' saturation and improving tractive and normal force estimations, through designing disturbance observers.

APPENDIX A
MATRICES FOR NORMAL FORCE APPROXIMATION

$$\mathbf{k} = \Psi^{-1} \begin{bmatrix} m_r g_u + 6w_w \\ (x_{cm} + L_0) m_r g_u + 2w_w(2L_0 + L) \\ (y_{cm} + c) m_r g_u + 6w_w c \\ (-\frac{1}{k_f} + \frac{L}{L_0 k_r} - \frac{L+L_0}{L_0 k_c}) w_w \\ 0 \\ (-\frac{1}{k_f} + \frac{L+L_0}{L_0 k_c} + \frac{1}{k_r} - \frac{L+L_0}{L_0 k_r}) w_w \end{bmatrix},$$

$$\Phi = \Psi^{-1} \begin{bmatrix} \mathbb{O}_{1\times 8} \\ -R_w \boldsymbol{\phi}_1^T \\ -R_w \boldsymbol{\phi}_2^T \\ \mathbb{O}_{3\times 8} \end{bmatrix}, \qquad \Pi = \Psi^{-1} \begin{bmatrix} \mathbb{O}_{1\times 7} \\ -\boldsymbol{\pi}_1^T \\ -\boldsymbol{\pi}_2^T \\ \mathbb{O}_{3\times 7} \end{bmatrix},$$

where the matrix Ψ is

$$\Psi = \begin{bmatrix} 1 & 1 & 1 & 1 & 1 & 1 \\ L_0 & L_0 & 0 & 0 & L+L_0 & L+L_0 \\ 2c & 0 & 2c & 0 & 2c & 0 \\ 0 & \frac{L+L_0}{L_0 k_c} & 0 & \frac{-L}{L_0 k_r} & 0 & -\frac{1}{k_f} \\ -\frac{1}{k_c} & \frac{1}{k_c} & \frac{1}{k_r} & -\frac{1}{k_r} & 0 & 0 \\ 0 & \frac{L+L_0}{L_0 k_c} & \frac{1}{k_r} & -\frac{L+L_0}{L_0 k_r} & -\frac{1}{k_f} & 0 \end{bmatrix}.$$

$$L_n = \begin{bmatrix} 0 & \frac{1}{2} & 0 & 0 & 1 & 0 & 0 & 0 \\ 0 & \frac{1}{2} & 0 & 0 & 0 & 1 & 0 & 0 \\ 0 & 0 & 0 & 0 & 0 & 0 & 1 & 0 \\ 0 & 0 & 0 & 0 & 0 & 0 & 0 & 1 \\ \frac{1}{2} & 0 & 1 & 0 & 0 & 0 & 0 & 0 \\ \frac{1}{2} & 0 & 0 & 1 & 0 & 0 & 0 & 0 \end{bmatrix}^T.$$

REFERENCES

[1] T. Peynot and S. Lacroix, "Enhanced locomotion control for a planetary rover," in *Proceedings 2003 IEEE/RSJ International Conference on Intelligent Robots and Systems (IROS 2003)(Cat. No. 03CH37453)*, vol. 1. IEEE, 2003, pp. 311–316.

[2] P. Niksirat, A. Daca, and K. Skonieczny, "The effects of reduced-gravity on planetary rover mobility," *The International Journal of Robotics Research*, vol. 39, no. 7, pp. 797–811, 2020.

[3] P. Kachroo and M. Tomizuka, "Vehicle traction control and its applications," 1994.

[4] D. Wang and C. B. Low, "Modeling and analysis of skidding and slipping in wheeled mobile robots: Control design perspective," *IEEE Transactions on Robotics*, vol. 24, no. 3, pp. 676–687, 2008.

[5] C.-F. Huang and T.-J. Yeh, "Anti slip balancing control for wheeled inverted pendulum vehicles," *IEEE Transactions on Control Systems Technology*, vol. 28, no. 3, pp. 1042–1049, 2020.

[6] H. A. Hashim and A. E. E. Eltoukhy, "Nonlinear filter for simultaneous localization and mapping on a matrix lie group using imu and feature measurements," *IEEE Transactions on Systems, Man, and Cybernetics: Systems*, pp. 1–12, 2021.

[7] K. Berntorp, "Joint wheel-slip and vehicle-motion estimation based on inertial, gps, and wheel-speed sensors," *IEEE Transactions on Control Systems Technology*, vol. 24, no. 3, pp. 1020–1027, 2016.

[8] M. Corno, G. Panzani, and S. M. Savaresi, "Traction-control-oriented state estimation for motorcycles," *IEEE Transactions on Control Systems Technology*, vol. 21, no. 6, pp. 2400–2407, 2013.

[9] P. Lamon and R. Siegwart, "3d position tracking in challenging terrain," *The International Journal of Robotics Research*, vol. 26, no. 2, pp. 167–186, 2007.

[10] Y. Zhou, H. Li, and L. Kneip, "Canny-vo: Visual odometry with rgb-d cameras based on geometric 3-d–2-d edge alignment," *IEEE Transactions on Robotics*, vol. 35, no. 1, pp. 184–199, 2019.

[11] Y. Zhou, G. Gallego, and S. Shen, "Event-based stereo visual odometry," *IEEE Transactions on Robotics*, vol. 37, no. 5, pp. 1433–1450, 2021.

[12] Z. Lei, P. Cui, H. Ju, and X. Peng, "Traction control on loose soil for a redundantly actuated mobile robot," in *International Conference on Intelligent Robotics and Applications*. Springer, 2008, pp. 1155–1164.

[13] Y. P. Li, M. H. Ang, and W. Lin, "Slip modelling, detection and control for redundantly actuated wheeled mobile robots," in *2008 IEEE/ASME International Conference on Advanced Intelligent Mechatronics*. IEEE, 2008, pp. 967–972.

[14] N. Sidek and N. Sarkar, "Dynamic modeling and control of nonholonomic mobile robot with lateral slip," in *Third International Conference on Systems (icons 2008)*. IEEE, 2008, pp. 35–40.

[15] D. Tavernini, M. Metzler, P. Gruber, and A. Sorniotti, "Explicit nonlinear model predictive control for electric vehicle traction control," *IEEE Transactions on Control Systems Technology*, vol. 27, no. 4, pp. 1438–1451, 2019.

[16] D. M. Helmick, S. I. Roumeliotis, Y. Cheng, D. S. Clouse, M. Bajracharya, and L. H. Matthies, "Slip-compensated path following for planetary exploration rovers," *Advanced Robotics*, vol. 20, no. 11, pp. 1257–1280, 2006.

[17] K. Noori and K. Jenab, "Fuzzy reliability-based traction control model for intelligent transportation systems," *IEEE Transactions on Systems, Man, and Cybernetics: Systems*, vol. 43, no. 1, pp. 229–234, 2013.

[18] R. Gonzalez, D. Apostolopoulos, and K. Iagnemma, "Improving rover mobility through traction control: simulating rovers on the moon," *Autonomous Robots*, vol. 43, no. 8, pp. 1977–1988, 2019.

[19] G. Huskić, S. Buck, M. Herrb, S. Lacroix, and A. Zell, "High-speed path following control of skid-steered vehicles," *The International Journal of Robotics Research*, vol. 38, no. 9, pp. 1124–1148, 2019.

[20] S. Wu, L. Li, Y. Zhao, and M. Li, "Slip ratio based traction coordinating control of wheeled lunar rover with rocker bogie," *Procedia Engineering*, vol. 15, pp. 510–515, 2011.

[21] T. Kawabe, M. Nakazawa, I. Notsu, and Y. Watanabe, "A sliding mode controller for wheel slip ratio control system," *Vehicle system dynamics*, vol. 27, no. 5-6, pp. 393–408, 1997.

[22] V. Ivanov, D. Savitski, and B. Shyrokau, "A survey of traction control and antilock braking systems of full electric vehicles with individually controlled electric motors," *IEEE Transactions on Vehicular Technology*, vol. 64, no. 9, pp. 3878–3896, 2014.

[23] N. Seegmiller, F. Rogers-Marcovitz, G. Miller, and A. Kelly, "Vehicle model identification by integrated prediction error minimization," *The International Journal of Robotics Research*, vol. 32, no. 8, pp. 912–931, 2013.

[24] E. Reichensdörfer, D. Odenthal, and D. Wollherr, "On the stability of nonlinear wheel-slip zero dynamics in traction control systems," *IEEE Transactions on Control Systems Technology*, vol. 28, no. 2, pp. 489–504, 2020.

[25] R. Gonzalez and K. Iagnemma, "Slippage estimation and compensation for planetary exploration rovers. state of the art and future challenges," *Journal of Field Robotics*, vol. 35, no. 4, pp. 564–577, 2018.

[26] K. Iagnemma and C. C. Ward, "Classification-based wheel slip detection and detector fusion for mobile robots on outdoor terrain," *Autonomous Robots*, vol. 26, no. 1, pp. 33–46, 2009.

[27] K. Iagnemma and S. Dubowsky, "Traction control of wheeled robotic vehicles in rough terrain with application to planetary rovers," *The international Journal of robotics research*, vol. 23, no. 10-11, pp. 1029–1040, 2004.

[28] P. Lamon and R. Siegwart, "Wheel torque control in rough terrain-modeling and simulation," in *Proceedings of the 2005 IEEE international conference on robotics and automation*. IEEE, 2005, pp. 867–872.

[29] N. Sarkar and X. Yun, "Traction control of wheeled vehicles using dynamic feedback approach," in *Proceedings. 1998 IEEE/RSJ International Conference on Intelligent Robots and Systems. Innovations in Theory, Practice and Applications (Cat. No. 98CH36190)*, vol. 1. IEEE, 1998, pp. 413–418.

[30] L.-Y. Hsu and T.-L. Chen, "An optimal wheel torque distribution controller for automated vehicle trajectory following," *IEEE transactions on vehicular technology*, vol. 62, no. 6, pp. 2430–2440, 2013.

[31] S. Barthelmes and U. Konigorski, "Model-based chassis control system for an over-actuated planetary exploration rover," *at-Automatisierungstechnik*, vol. 68, no. 1, pp. 58–71, 2020.

[32] H. Guo, Z. Yin, D. Cao, H. Chen, and C. Lv, "A review of estimation for vehicle tire-road interactions toward automated driving," *IEEE Transactions on Systems, Man, and Cybernetics: Systems*, vol. 49, no. 1, pp. 14–30, 2019.

[33] B. H. G. Barbosa, N. Xu, H. Askari, and A. Khajepour, "Lateral force prediction using gaussian process regression for intelligent tire systems," *IEEE Transactions on Systems, Man, and Cybernetics: Systems*, pp. 1–12, 2021.

[34] M. Mottaghi and R. Chhabra, "Robust optimal output-tracking control of constrained mechanical systems with application to autonomous rovers," *IEEE Transactions on Control Systems Technology*, 2022.

[35] G. Campion, G. Bastin, and B. Dandrea-Novel, "Structural properties and classification of kinematic and dynamic models of wheeled mobile robots," *IEEE Transactions on Robotics and Automation*, vol. 12, no. 1, pp. 47–62, 1996.

[36] M. Mottaghi, "Optimal robust output-tracking of autonomous rovers with dynamic traction control," Master's thesis, Carleton University, 2022.

[37] D. Wang and G. Xu, "Full-state tracking and internal dynamics of nonholonomic wheeled mobile robots," *IEEE/ASME Transactions on mechatronics*, vol. 8, no. 2, pp. 203–214, 2003.

[38] G. Strang, G. Strang, G. Strang, and G. Strang, *Introduction to linear algebra*. Wellesley-Cambridge Press Wellesley, MA, 1993, vol. 3.

[39] D. P. Bertsekas, "Nonlinear programming," *Journal of the Operational Research Society*, vol. 48, no. 3, pp. 334–334, 1997.

[40] "Vortex studio release 6.8.1," CM Labs Simulations Inc., Montreal, Canada., Tech. Rep.

[41] A. Peiret, E. Karpman, L. L. Kovács, J. Kövecses, D. Holz, and M. Teichmann, "Modelling of off-road wheeled vehicles for real-time dynamic simulation," *Journal of Terramechanics*, vol. 97, pp. 45–58, 2021.

M.R Mottaghi was born in Esfahan, Esfahan, Iran in 1996. He received the B.S. degree in mechanical engineering from Isfahan University of Technology,Esfahan, Iran, in 2019. Then, he joined Autonomous Space Robotics and Mechatronics Lab (ASRoM Lab) at Carleton University, Ottawa, ON, Canada to pursue his M.A.Sc degree in mechanical engineering in 2019. Since 2019, he has been working as a Research Assistant with ASRoM Lab. His research interests include, robust control design, nonholonomic mechanics, and traction control.

Robin Chhabra (IEEE Member) is a Tier-II Canada Research Chair in autonomous space robotics and mechatronics at Carleton University. His team is focused on developing methodologies for the long-term, intelligent autonomy of space robotic systems. Dr. Chhabra received his M.A.Sc. (2008) and Ph.D. (2013) from the University of Toronto Institute for Aerospace Studies. After a postdoctoral fellowship at the University of Calgary, he joined MacDonald Dettwiler and Associates Ltd., where he focused on applied research on the control of space systems. Dr. Chhabra's research interest include applications of geometric mechanics, nonlinear controls, and artificial intelligence, in the control of robotic systems.

Fast Traction Control of Rovers on Prescribed Dynamic Trajectories with Wheel-Fighting Consideration

Mohammadreza Mottaghi, Robin Chhabra, *Member, IEEE*, Wei Huang

I. Suplementary Materials

A. Validation of Normal and Tractive Force Approximations

The validity of the approximated tractive and normal forces is demonstrated by developing a software-in-the-loop simulation environment using Vortex Studio 2020b. This simulation contains the controller coded in MATLAB Simulink connected to a digital twin of the Lunar rover modeled in Vortex Studio. Fig.1 depicts the designed mechanism in Vortex.

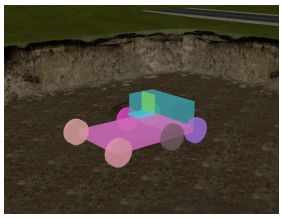

Fig. 1: The designed mechanism in Vortex

The stiffness of the suspension springs are shown in Table.I. The amount of damping coefficients for the suspension system are designed to be 10KNs/m, 15KNs/m, and 20KNs/m for front, center and rear wheels, respectively. These values are selected based on the realistic coefficients used in the suspension system of off-road vehicles, with similar weights. The considered wheel-soil interaction model is generated based on the box model of dry friction cone, where lateral and longitudinal friction coefficients are independent. For simplicity, the rolling resistance at all wheels and the lateral friction at rear wheels are equated to zero. Accordingly, system is not subject to any sources of disturbances, except for those coming from the force distribution at the wheel-ground contact patches, according to the applied tire model. The values of kinematic and dynamic parameters used in the model along with controller gains are depicted in Table.I.

The approximated normal and tractive forces are compared with the actual values outputted from Vortex. For simplicity, this comparison is performed when the uniform control distribution is applied, i.e. $\boldsymbol{\tau}_a = 0$. It is also noteworthy that the default values in Vortex are considered for the tire deformation and wheels' damping.

M.R. Mottaghi and R. Chhabra are with the Mechanical and Aerospace Engineering department, Carleton University, Ottawa, Canada (e-mail: mohammadreza.mottaghi@carleton.ca, robin.chhabra@carleton.ca. W.Huang is with National Research Council of Canada (NRC-CNRC) AST center, Ottawa, Canada (e-mail: Wei.Huang@nrc-cnrc.gc.ca)

Rover Parameters			
L[m]	L_0[m]	c[m]	R_w[m]
1	0.5	0.55	0.2
l[m]	x_{cm}[m]	y_{cm}[m]	m_r[Kg]
1	0.05	0	600
m_w[Kg]	J_r[Kg/m^2]	J_{wy}[Kg/m^2]	J_{wz}[Kg/m^2]
40	450	1	1
g_u[m/s^2]	k_f[N/m]	k_c[N/m]	k_r[m/s]
1.632	30000	45000	60000
Controller Gains			
K_p	K_I	K_d	
48	64	12	

TABLE I: Lunar rover's model and controller parameters.

The considered desired trajectory for the system is moving on a straight line for the first 30s with a forward velocity profile containing periodic acceleration deceleration phases with time varying magnitude. The equation of this velocity profile is $0.4t\sin\left(\frac{4\pi}{30}\right)^2$m/s. Then, system accelerates with the constant acceleration of 0.3m/s^2 for 8s and continues its motion with a constant velocity until 55^{th} second of the simulation. At 40^{th} second a fast steering command is applied in the form of a trapezoidal velocity profile and system starts circling. At 55^{th} second we apply a brake command with the constant acceleration -0.05 m/s^2 for five seconds. After circling with the reduced constant velocity for another 5s, we apply a constant acceleration command with the magnitude equal to 0.05m/s^2 for 10s. Afterwards, system continues with increased constant velocity for the rest of the simulation time. This desired trajectory is demonstrated in Fig. 2.

Remark 1. This trajectory is designed to evaluate the validity of the normal/tractive force approximations while system performs different maneuvers including acceleration/deceleration on both a straight line and a circular path, sharp steering, and traction loss in the longitudinal direction. Since, traction loss in the lateral direction leads to a complete drift from the desired trajectory and misrepresentation of the intended validation, it is tried to keep system away from such a condition during designing the trajectory while the uniform control distribution is applied.

The comparison of the estimated normal forces and actual values at all wheels is shown in Fig. 3 and the comparison of the estimated longitudinal tractive forces and actual values are depicted in Fig. 4. Such a comparison for the lateral tractive forces is also shown in Fig. 5. During motion on the straight line the approximated values of the normal forces acceptably match the actual ones. However, a small

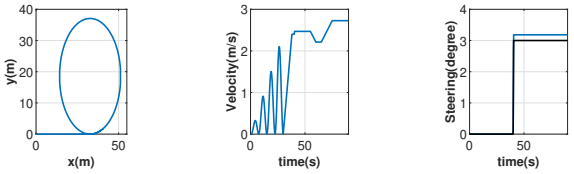

(a) (b) (c)

Fig. 2: Desired trajectory: (a) desired path (b) desired forward velocity of the rover (c) desired steering angles

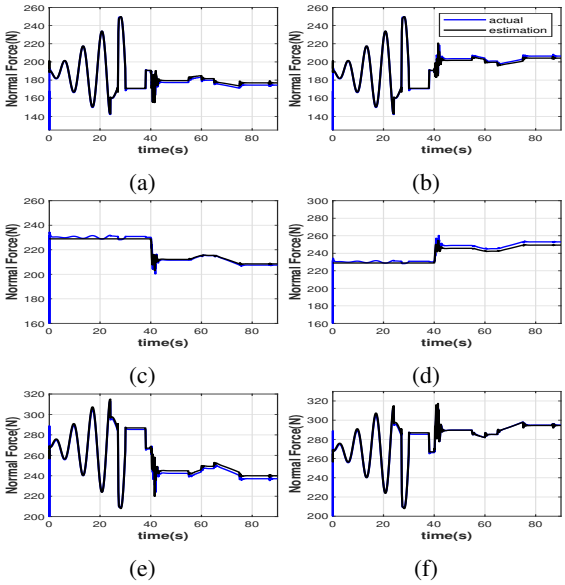

(a) (b) (c) (d) (e) (f)

Fig. 3: Validation of approximated normal forces. (a) correspond to port front, (b) starboard front, (c) port center, (d) starboard center, and (e) and (f) correspond to port and starboard rear wheels, respectively.

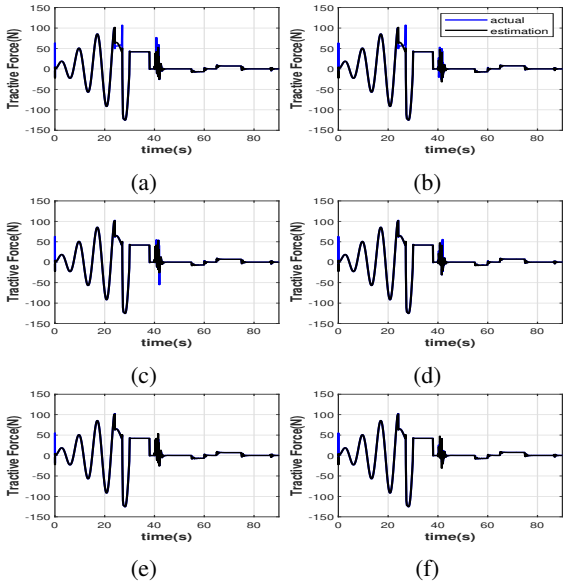

(a) (b) (c) (d) (e) (f)

Fig. 4: Validation of approximated longitudinal tractive forces. (a) correspond to port front, (b) starboard front, (c) port center, (d) starboard center, and (e) and (f) correspond to port and starboard rear wheels, respectively.

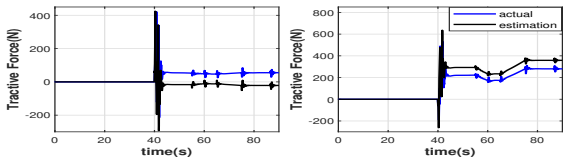

(a) (b)

Fig. 5: Validation of approximated lateral tractive forces using default tire deformation. (a) at front (b) at center wheels.

discrepancy can be observed in these approximations due to unmodelled dynamics of suspension system. When the system starts turning, the distribution of the normal forces at the tire contact patches becomes asymmetric that results in generating an excess torque in roll direction. Accordingly, a slight offset between the actual values and the estimated values during circling can be observed. Concerning the longitudinal tractive forces, we have an acceptable match except for the 24^{th} and 40^{th} seconds of the simulation. At those instances, the system under uniform control distribution initiates the dynamic friction regime at some of the wheels. Consequently, the nonholonomic constraint equations are no longer valid, which justifies the observed discrepancy. The maximum percentage error of the approximations, excluding the time in which system experiences dynamic friction, are $3.5\%, 1.45\%$, and 2.27% for normal forces respectively at front, center and rear wheels, along with $7.2\%, 1.40\%$, and 1.41% for longitudinal tractive forces respectively at front, center and rear wheels.

Although the approximation of the lateral tractive forces captures the trend of actual values, but in reality such forces are distributed differently between different axles. The reason behind this observation is the distribution of tractive forces at the tire contact patches which are not considered in our approximation. Such distributions produce considerable amount of torques in the yaw direction, resulting in an offsetted distribution of the lateral tractive forces between the front and center axles. To address this discrepancy we must either use a tire model in our approximation or decrease the tire deformation.